Human Molecular Genetics, 2020, Vol. 29, No. 20 3373–3387

doi: 10.1093/hmg/ddaa228
Advance Access Publication Date: 19 October 2020
General Article

GENERAL ARTICLE

Nf2 fine-tunes proliferation and tissue alignment during closure of the optic fissure in the embryonic mouse eye

Wesley R. Sun[1,‡], Sara Ramirez[1,2,‡], Kelly E. Spiller[1], Yan Zhao[1] and Sabine Fuhrmann[1,2,*,†]

[1]Department of Ophthalmology and Visual Sciences, VEI, Vanderbilt University Medical Center, Nashville, TN 37232, USA and [2]Department of Cell and Developmental Biology, Vanderbilt University School of Medicine, Nashville, TN 37240, USA

*To whom correspondence should be addressed at: Department of Ophthalmology and Visual Sciences, Vanderbilt University Medical Center, 1161 21st Ave S, AA7100 MCN (in VUIIS), Vanderbilt Eye Institute Research Laboratories, Nashville, TN 37232, USA. Tel: +1 6159360621; Fax: +1 6159366410; Email: sabine.fuhrmann@vanderbilt.edu

Abstract

Uveal coloboma represents one of the most common congenital ocular malformations accounting for up to 10% of childhood blindness (~1 in 5000 live birth). Coloboma originates from defective fusion of the optic fissure (OF), a transient gap that forms during eye morphogenesis by asymmetric, ventral invagination. Genetic heterogeneity combined with the activity of developmentally regulated genes suggests multiple mechanisms regulating OF closure. The tumor suppressor and FERM domain protein Neurofibromin 2 (NF2) controls diverse processes in cancer, development and regeneration, via Hippo pathway and cytoskeleton regulation. In humans, *NF2* mutations can cause ocular abnormalities, including coloboma, however, its actual role in OF closure is unknown. Using conditional inactivation in the embryonic mouse eye, our data indicate that loss of *Nf2* function results in a novel underlying cause for coloboma. In particular, mutant eyes show substantially increased retinal pigmented epithelium (RPE) proliferation in the fissure region with concomitant acquisition of RPE cell fate. Cells lining the OF margin can maintain RPE fate ectopically and fail to transition from neuroepithelial to cuboidal shape. In the dorsal RPE of the optic cup, *Nf2* inactivation leads to a robust increase in cell number, with local disorganization of the cytoskeleton components F-actin and pMLC2. We propose that RPE hyperproliferation is the primary cause for the observed defects causing insufficient alignment of the OF margins in *Nf2* mutants and failure to fuse properly, resulting in persistent coloboma. Our findings indicate that limiting proliferation particularly in the RPE layer is a critical mechanism during OF closure.

Introduction

Congenital ocular malformations such as anophthalmia, microphthalmia and coloboma (MAC) are the cause for over 25% of childhood blindness worldwide (1–3). Uveal coloboma alone may account for up to 10% of childhood blindness, ~1 in 5000 live birth (4,5) for reviews, see (6–8); it is most commonly observed as missing tissue in the ventro-nasal region of the eye and

†Sabine Fuhrmann, http://orcid.org/0000-0002-2456-5490
‡The authors wish to be known that, in their opinion, the first two authors Wesley R. Sun and Sara Ramirez should be regarded as joint first authors.
Received: June 17, 2020. **Revised:** September 29, 2020. **Accepted:** October 12, 2020

originates from a failure in apposition and fusion of the margins of the optic fissure (OF). The OF forms as a ventral groove by asymmetric invagination, extending from the vitreal side to the proximal junction with the forebrain that allows mesenchymal cells to migrate in and form the hyaloid vessel (9–11). Closure of the OF occurs when mesenchymal cells end migration; the laterally growing edges of the retinal pigmented epithelium (RPE) and retina cells lining the OF margins appose to fuse and form a continuous optic cup. Fusion starts at the midpoint of the OF and moves in both directions distally and proximally (9,12). The etiology of coloboma is complex, and defects result from disturbance of heterogenous genetic and/or environmental factors suggesting multiple mechanisms in regulating the closure process, including cell autonomous and cell non-autonomous tissue interactions. In humans, a subpopulation of colobomata is a result of mutations in developmentally important genes; however, the origins for many OF closure defects are unknown (for reviews, see 3,7,8,13,14). Additional genes have been identified in animal models; substantial progress has been made in understanding critical processes, including growth and patterning of the ventral optic cup and optic nerve head (15–19), cell-cell contact and signaling (20–30), crosstalk with migrating hyaloid precursors and extracellular matrix components (31–36), cytoskeleton dynamics (37,38), epigenetics (39), degradation of ECM and cellular proteins (40–42), programmed cell death, survival and cell proliferation (43,44) (for reviews, see 7,8,13). Elegant *in vivo* imaging studies in zebrafish and excellent anatomical analyses in chick have characterized important morphogenetic and cellular behavior (20,27,34,45–49). In addition, comprehensive gene expression analyses have identified novel candidate genes potentially relevant for regulating OF closure (27,47,50–52).

Gene mutations of Hippo signaling pathway components represent novel associations with coloboma (7,23,53,54). Mutations in the Neurofibromin 2 (*NF2*) gene result in the autosomal dominant disorder Neurofibromatosis Type 2 (NF2, OMIM # 101000), a relatively rare syndrome characteristic of neoplastic lesions. Human *NF2* mutations associate frequently with ocular abnormalities (53,55–57). Importantly, some patients with loss of *NF2* heterozygosity also exhibit coloboma, consistent with *Nf2* being identified as a coloboma gene in mouse (53,58,59) (this study). The *Nf2* gene encodes the FERM (4.1 protein/Ezrin/Radixin/Moesin) domain protein MERLIN. It exerts multiple functions in tumor suppression, development and regeneration in diverse organs and tissues, for example by restricting proliferation, controlling apoptosis, and promoting differentiation, apicobasal polarity and junctional complex formation (60–62). NF2 localizes primarily to the cell cortex and links the cortical actomyosin cytoskeleton to the plasma membrane. It associates with α-catenin to promote establishment of intercellular junctions and polarity complexes (63). In addition, NF2 can localize to the nucleus and act as a contact-dependent tumor suppressor by inhibiting CRL4DCAF1 ubiquitin ligase (61). Importantly, among other regulatory inputs, NF2 also controls the Hippo pathway to balance organ size, proliferation and behavior of stem cells; it binds to and activates several Hippo pathway components, including the Hippo kinases MST1/2 and LATS1/2 (61,62). Loss of Hippo signaling leads to nuclear translocation of the transcriptional co-activators YAP/TAZ, often associated with abnormal proliferation in cancer and during development. Human mutations of *YAP* and its transcriptional effector *TEAD* can result in coloboma and the autosomal dominant ocular disorder Sveinsson's chorioretinal atrophy, respectively (SCRA, OMIM # 108985) (54,64,65). Recent studies in Drosophila, zebrafish and mouse elucidate functions of Yap/Taz during ocular development, with some aspects of evolutionary conservation (59,66–71) (for reviews, see 72–74).

Our study focuses on the role of Nf2 during OF closure in mouse. NF2 protein is expressed in developing ocular tissues and is required for development of the lens and the optic cup, particularly of the ciliary margin into ciliary body and iris (58,59,75–77). Coloboma occurs upon tissue-specific *Nf2* deletion (58,59), however, it is unclear how loss of *Nf2* function affects the closure process. Our data demonstrate that *Nf2* disruption results in ectopic proliferation in the RPE layer in the OF region with concomitant maintenance of RPE cell fate. RPE cells in the temporal OF margin maintain columnar organization instead of transitioning to cuboidal shape. In the dorsal RPE of the optic cup, *Nf2* loss of function leads to a substantial increase in cell number, accompanied with local disorganization of cytoskeleton components F-actin and pMLC2. We propose that these abnormalities in the *Nf2* mutant optic cup cause insufficient alignment of the OF margins, resulting in a failure to attach and fuse properly, and, thus, leading to a persistent coloboma. Our analysis provides novel insights into the underlying mechanisms during OF closure as well as into the specific function of Nf2 in this process.

Results

Loss of *Nf2* function leads to a narrow coloboma in the ventral optic cup

Germline disruption of the *Nf2* gene causes early embryonic lethality before eye development commences (78). Therefore, we conditionally disrupted *Nf2* using *Rx3-Cre* that is constitutively active in the early optic vesicle starting at E8.75 and later in the optic cup in the presumptive retina, RPE and lens vesicle (77,79,80). OF closure starts at E10.5 and is completed by E12.5, evident by continuous pigmentation in the ventral optic cup at E13.5 (Fig. 1A and C). *Rx3-Cre*-mediated, conditional ablation of *Nf2* (hereafter $Nf2^{CKO}$) results in failure of OF fusion in both eyes of each embryo (E13.5–E17.5; Fig. 1B and D; $n = 22$). In $Nf2^{CKO}$ optic cups, the OF margins are tightly apposed, suggesting a defect during the final process of closing (Fig. 1D). Persistent expression of laminin in the central ventral optic cup confirms failed degradation of the basement membrane between the OF margins (Fig. 1F; see Supplementary Material, Fig. S1A for sagittal section scheme). We did not observe any coloboma in conditional heterozygous embryos (not shown). Laminin persistence in $Nf2^{CKO}$ shows 100% penetrance in the distal optic cup, close to the ciliary margin, while some can exhibit laminin degradation proximally at E13.5 (33%, 3/9 eyes, $n = 7$). Thus, coloboma in $Nf2^{CKO}$ eyes is less likely to be a delay in timing since failed closure in the distal, and frequently in the proximal region of the optic cup, is persistent at later stages. Compared with controls, the RPE layer in $Nf2^{CKO}$ eyes appears slightly darker (Fig. 1D and H; Supplementary Material, Fig. S1C) and increased in height (Fig. 1G and H; insets). In addition, $Nf2^{CKO}$ embryos display additional, fully penetrant tissue fusion defects in closure of eye lids, lip and palate, as previously observed (Fig. 1B; not shown) (58).

A 2.4 kB human *NF2* promoter element was recently identified to generate a *NF2-lacZ* reporter mouse, showing robust activation specifically in the RPE between E10.5 and E12.5 (81). NF2 protein is transiently expressed in the retina and continuously present in RPE and ciliary margin (59,75). *Nf2* reporter activation and NF2 protein expression in the eye matches expression of the Hippo pathway target YAP. YAP1 protein normally shows

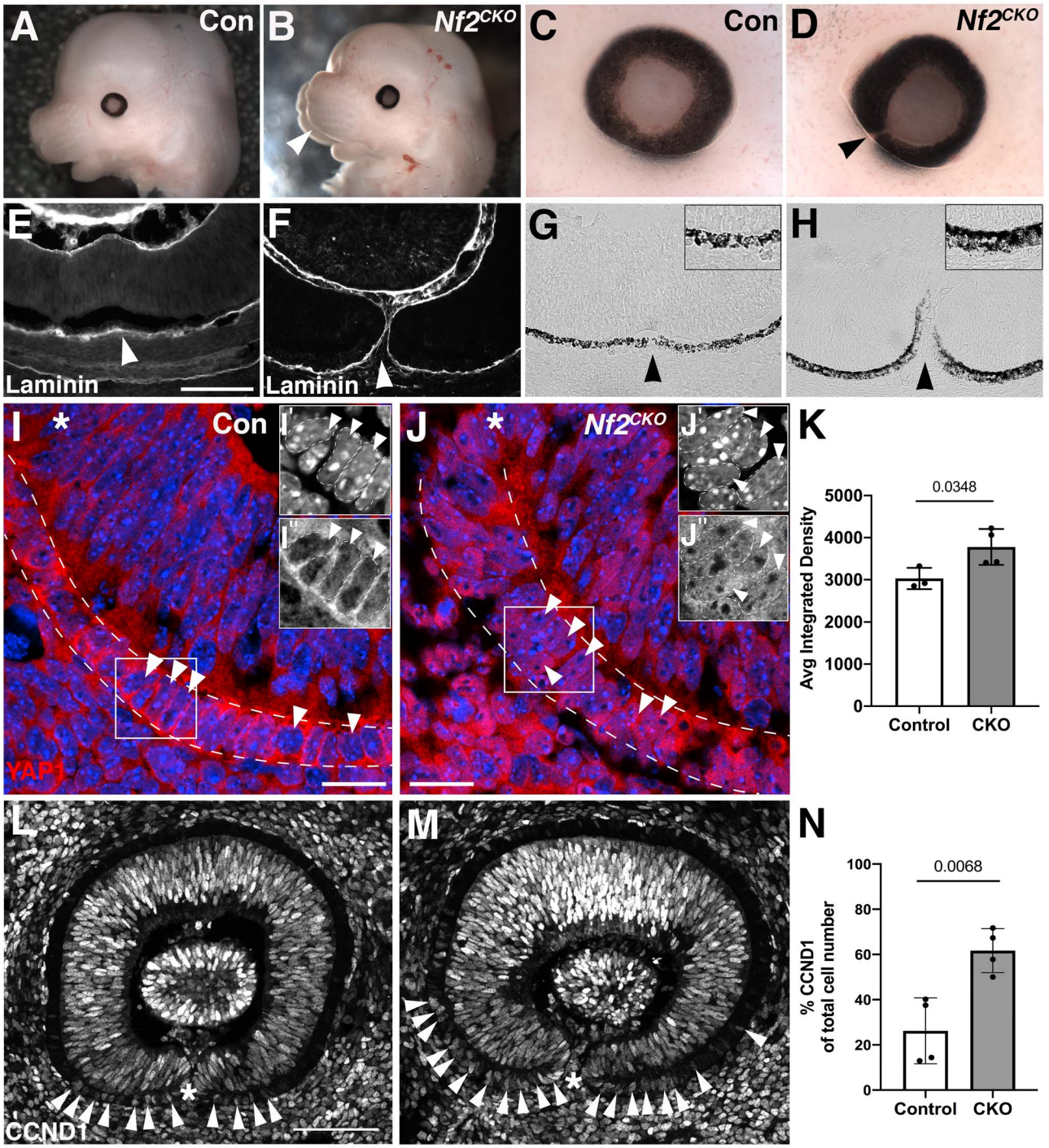

Figure 1. Nf2 disruption in ocular tissues causes coloboma in the embryonic mouse eye. (**A**) Control embryonic head at E13.5. (**B**) *Nf2*^{CKO} embryos exhibit cleft lip and palate (arrowhead). (**C**) Higher magnification of E13.5 control eye. (**D**) In *Nf2*^{CKO} embryos at E13.5, the ventral eye shows an OF closure defect with a narrow gap (arrowhead) and the pigment appears slightly darker. (**E**) Immunolabeling for the basement marker laminin in the E13.5 ventral optic cup of controls confirms absence of laminin and successful fusion of the OF region (arrowhead). Sagittal view with nasal orientation to the left. (**F**) Laminin is persistent in the ventral optic cup in E13.5 *Nf2*^{CKO} embryos indicating failed OF fusion (arrowhead). (**G**) Brightfield image of the ventral optic cup in control showing pigmentation of the RPE in the fused OF (arrowhead). (**H**) In the ventral optic cup of E13.5 *Nf2*^{CKO} embryos, pigmentation extends into the unfused OF (arrowhead) and the RPE layer appears slightly increased in height. Insets in G, H show magnified regions outlined in boxed area, revealing increased thickness in mutant RPE (H). (**I**) During OF closure at E11.5, YAP1 protein expression can be localized both to the cytoplasm and nucleus in the RPE (arrowheads point to RPE nuclei). (**J**) In *Nf2*^{CKO} eyes, nuclear YAP1 expression can be increased in retina and RPE (arrowheads display nuclear Yap localization in RPE). RPE in I and J is indicated by dotted lines and sections were counterstained with 2-(4-amidinophenyl)-1H-indole-6-carboxamide (Dapi, blue). Insets in I and J show enlarged greyscale images of individual cells in the RPE (boxed area). I′ and J′ display the Dapi channel, I″ and J″ display the YAP1 channel. Individual nuclei in the insets are outlined by dotted lines. (**K**) YAP1 average integrated density per RPE nuclei shows a significant increase in *Nf2*^{CKO} compared with control nuclei. (**L**, **M**) Cyclin D1 (CCND1)-labeled cells are significantly increased in *Nf2*^{CKO} ventral RPE (M; arrowheads; **N**). Asterisks in I, J, L, M indicate OF. Data are shown as means ± SD, and *P*-values are indicated above the horizontal lines in each graph (significant < 0.05). Statistical analysis was performed using unpaired, two-tailed Student *T*-test (Welch's correction included for K). Scale bars: 100 µm in E, L; 20 µm in I, J.

cytoplasmic and nuclear localization in developing ocular tissues and in adjacent periocular mesenchyme (54,59,68,72,82,83). Consistent with previous studies, we observed YAP1 expression in the cytoplasm and nucleus in retina and RPE during OF closure (Fig. 1I, insets I′–I″ Supplementary Material, Fig. S1F and M). In $Nf2^{CKO}$ optic cups, nuclear localization of YAP can be increased in cells of the RPE, as well as in retina and lens (Fig. 1J, insets J′–J″; Supplementary Material, Fig. S1I and N; E11.0–E11.5; $n = 9$). We quantified nuclear YAP signal intensity, confirming a significant increase in RPE cells adjacent to the OF as well as in the retina of $Nf2^{CKO}$ compared with controls (Fig. 1K; Supplementary Material, Fig. S1K). Additionally, we calculated area of nuclei and observed no significant difference in the RPE and retina of control and $Nf2^{CKO}$ in E11.5 optic cups (Supplementary Material, Fig. S1J and L). The ventral RPE layer in $Nf2^{CKO}$ can appear increased in thickness, possibly due to an increase in cell number and cellular crowding (Supplementary Material, Fig. S1G–I; see also below Fig. 4). In addition, we investigated expression the cell cycle regulatory protein cyclin D1, a direct transcriptional target of YAP/TEAD in other tissues (84). We observed that in mutant RPE, significantly more cells express cyclin D1 in the ventral optic cup (Fig. 1M and N). Thus, our data strongly suggest that Nf2 function is required for retention of (phosphorylated) YAP in the cytoplasm during OF closure.

In the ventral optic cup of $Nf2^{CKO}$, RPE markers persist in the OF

Loss of *Nf2* results in increased nuclear YAP localization (Fig. 1), and YAP is required and sufficient to control RPE cell fate in zebrafish and mouse (67,68). Therefore, we analyzed retina and RPE markers in the OF region between E11.5 and E13.5, during and after OF alignment and fusion, respectively (Fig. 2). The expression patterns of the pan-ocular paired PAX6 transcription factor ($n = 3$) and retina-specific VSX2 homeodomain transcription factor ($n = 4$) are unchanged in the ventral optic cup of $Nf2^{CKO}$ embryos at E11.5 (Fig. 2B and D). Dorsal localization of the T-box transcription factor TBX5 is unaltered in the $Nf2^{CKO}$ optic cup (Fig. 2F; $n = 4$, E11.5–E13.5) (85). Similarly, ventral expression of the paired homeodomain transcription factor PAX2, essential for OF closure, is robust in the OF margins in $Nf2^{CKO}$ (Fig. 2H). Therefore, general tissue patterning of retina and dorsoventral regionalization is not affected by loss of *Nf2* function.

The bicoid transcription factor Otx2 is required for RPE cell fate and RPE differentiation at the advanced optic vesicle stage (86,87). We observed that expression of OTX2 is ectopically maintained in the OF in several E11.5 $Nf2^{CKO}$ embryos (Fig. 2J; arrows; 57%; $n = 7$). At E13.5 all analyzed eyes showed persistent OTX2 expression in the OF (Fig. 2L; arrows; 100%; $n = 4$), consistent with extended pigmentation into the OF (Fig. 1D and H; Supplementary Material, Fig. S1C). The bHLH transcription factor MITF, a critical key regulatory factor for RPE cell fate and OF closure (18,88,89) is normally present in the approaching OF margins at E11.0 (Supplementary Material, Fig. S2A; arrows) and becomes progressively excluded ventrally during closing at E11.5 (Fig. 2M). At E11.0, MITF protein shows normal localization in the mutant OF (Supplementary Material, Fig. S2B; $n = 4$). However, at E11.5, MITF-labeled cells extend into the lower (ventral) OF in $Nf2^{CKO}$ optic cups (Fig. 2N; arrows; 100%; $n = 4$), suggesting persistent presence of RPE precursors in the OF. Abnormally upregulated RPE fate in the OF due to FGF pathway deficiency leads to failed OF fusion and YAP can cooperate with Pax transcription factors to promote MITF expression in neural crest progenitors (90–92). Therefore, to test whether excessive *Mitf* dosage in the OF margins is preventing OF closure, we removed one functional *Mitf* allele by crossing the $Mitf^{Mi}$ allele into $Nf2^{CKO}$ (89). Normally, heterozygous $Mitf^{Mi/+}$ optic cups are less pigmented (Supplementary Material, Fig. S2D). In $Nf2^{CKO}$;$Mitf^{Mi/+}$ optic cups, pigmentation is strongly reduced at E13.5, however, coloboma is still apparent (Supplementary Material, Fig. S2F and H; $n = 2$). Thus, loss of *Nf2* function can result in maintenance of RPE cell fate in the OF margins, however, it may not be the primary cause for defective OF closure in $Nf2^{CKO}$ eyes.

Wnt/β-catenin signaling and apicobasal polarity are unaltered upon loss of Nf2

Others and we have shown that Wnt/β-catenin signaling is required and sufficient for MITF and OTX2 expression in the mouse optic cup, and RPE-specific β-catenin gene disruption causes coloboma (93–96). However, gain of function of the pathway by disruption of the Wnt/β-catenin inhibitor *Axin2* can also result in coloboma, with persistent expression of MITF and OTX2 (19) similarly to $Nf2^{CKO}$. Importantly, several studies have shown that NF2 can associate with LRP6 and block its phosphorylation resulting in inhibition of Wnt/β-catenin pathway activation (97). To determine whether Wnt/β-catenin pathway activity is hyperactivated upon loss of Nf2 function, we utilized a knock-in $Axin2^{LacZ}$ reporter (98). We did not detect obvious changes in $Axin2^{LacZ}$ (β-GAL) expression in $Nf2^{CKO}$ heterozygous for $Axin2^{LacZ}$ (Fig. 2P; $n = 5$). Additionally, expression of the downstream effector and target LEF1 as an additional readout for pathway activity was not altered (Supplementary Material, Fig. S2I and J; $n = 4$). These data indicate that Wnt/β-catenin pathway activity is not restrained by *Nf2* function.

NF2 participates in assembly of plasma membrane protein complexes and couples them with the cortical actin cytoskeleton (58,60,61,63). In medaka, reduction of YAP results in decreased tension of the actomyosin network in embryonic tissues (99). Therefore, we reasoned that increased nuclear YAP may promote actomyosin activity in $Nf2^{CKO}$ ventral optic cups. Phosphorylated myosin light chain II (pMLC2) is normally localized to the apical RPE surface in the optic cup (Fig. 3A) (95,100). In the mutant ventral RPE, adjacent to the OF, we observed no obvious changes in apical localization of pMLC2 protein (Fig. 3B; $n = 3$). Similarly, localization of ZO-1, indicative for intercellular apical junction formation between retina and RPE, is not altered in $Nf2^{CKO}$ (Fig. 3D; $n = 5$). NF2 also regulates assembly of adherens junctions (AJ) in the mouse epidermis, linking it to polarity protein complexes (63). However, we observed no change in the distribution of the AJ core protein α-catenin in the OF and apical surfaces (Fig. 3E and F; $n = 3$). In addition, F-Actin localization in the ventral optic cup of $Nf2^{CKO}$ appears normal (Fig. 6B and D; E11.0–E11.5; $n = 7$). Thus, loss of *Nf2* in the optic vesicle does not interfere with apicobasal polarity, formation of adherens/tight junctions or actomyosin organization in the ventral optic cup during closure of the OF.

During OF closure, ventral RPE proliferation is abnormally increased in $Nf2^{CKO}$ eyes

Depending on the species, OF closure is tightly regulated by a balance of programmed cell death (apoptosis) and proliferation. In zebrafish, apoptosis is not abundant in the ventral optic cup, and cell death or proliferation are not required for OF closure (27,34,46,101,102). In chick and mammals, retinal apoptosis is prevalent and retinal proliferation is decreased in the vicinity of the OF margins during closure (9,10,27,103–105). Accordingly,

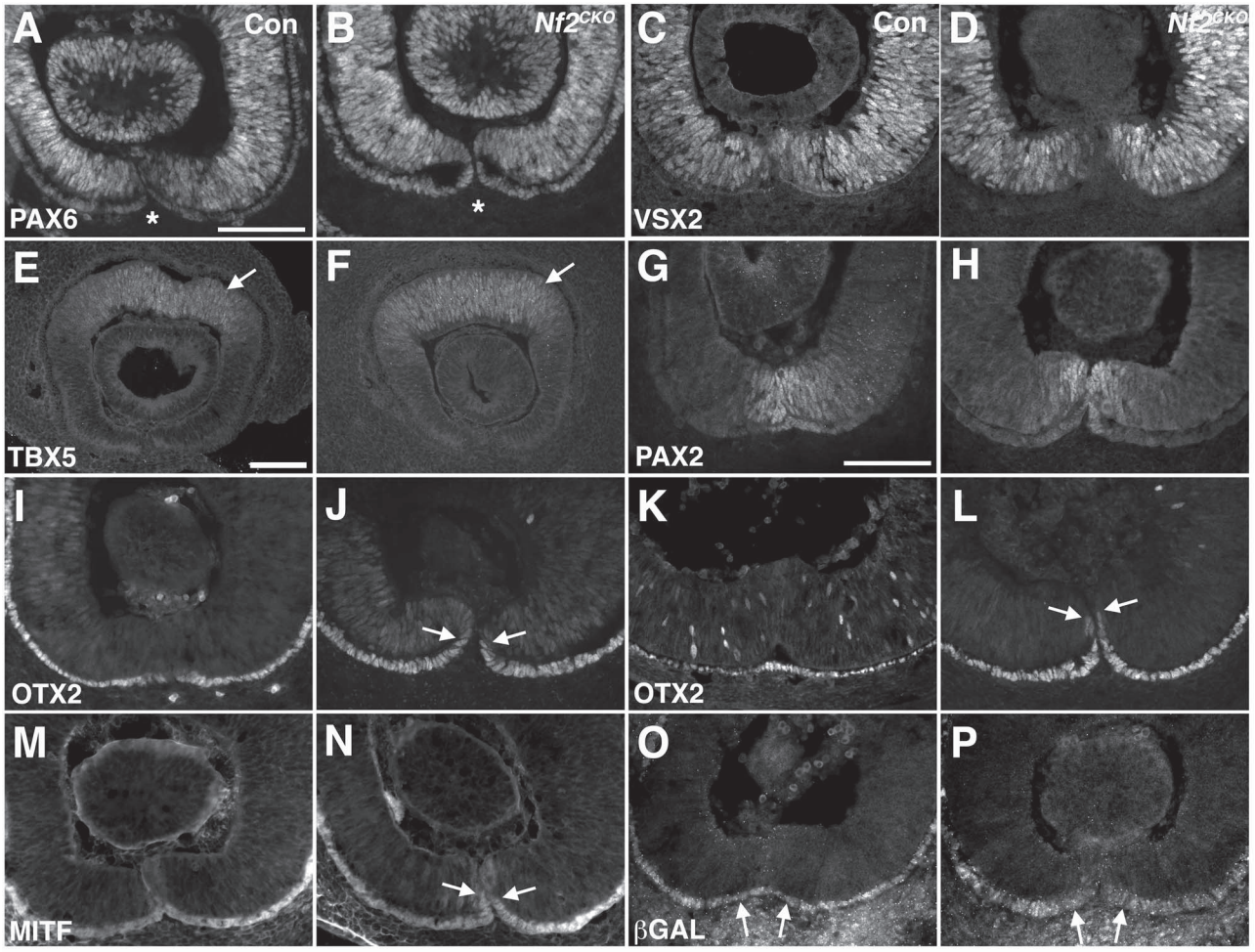

Figure 2. Analysis of tissue patterning in the $Nf2^{CKO}$ optic cup reveals persistence of RPE markers in the open OF. (**A–J**, **M–P**: E11.5; **K**, **L**: E13.5) A, B: Expression of the pan-ocular protein PAX6 is unaltered in $Nf2^{CKO}$ eyes (B). Asterisks label overlying OF. C, D: The retina-specific homeodomain protein VSX2 is normally expressed in $Nf2^{CKO}$ eyes (D). E, F: Analysis of TBX5 expression shows normal patterning of the dorsal optic cup in $Nf2^{CKO}$ embryos (F; arrow). G, H: In the ventral $Nf2^{CKO}$ optic cup, the key transcription factor PAX2 is normally localized (H). I, J: Expression of the RPE determination transcription factor OTX2 can be maintained in the open fissure of $Nf2^{CKO}$ eyes (J, arrows). K, L: At E13.5, coloboma is persistent in $Nf2^{CKO}$ embryos and the margins of the unclosed OF are lined with OTX2-positive cells (L, arrows). M, N: The bHLH transcription factor MITF is present in the RPE layer of the optic cup (M). In $Nf2^{CKO}$ embryos, MITF localization extends into the OF (N; arrows). O, P: Axin2 reporter expression, a readout for Wnt/β-catenin pathway activation, is not altered in the ventral RPE in $Nf2^{CKO}$ optic cups (arrows). Sagittal view with nasal orientation to the left. Scale bars: 100 μm in A, E, G.

abnormal changes in cell number by altered cell death or cell divisions in the optic cup can result in OF closure defects and colobomata (44,106). Since *Nf2* disruption causes altered apoptosis during neural tube closure (58), we first analyzed programmed cell death using TUNEL labeling. In the ventral optic cup of E11.5 $Nf2^{CKO}$ embryos, apoptosis was not significantly altered in the ventral quadrant harboring the OF (V2; Supplementary Material, Fig. S3A–D; see Supplementary Material, Fig. S3C for subdivision scheme). Nuclear localization of YAP can stimulate cell division, and a significant increase in RPE marker-labeled cells and BrdU incorporation in the RPE layer is observed in $Nf2^{CKO}$ using *Nestin-Cre* (58,59). However, spatial and temporal information critical for the process of OF closure is lacking; these studies were performed after completion of OF closure, and not regionally correlated with the OF. Thus, we performed a detailed proliferation analysis in $Nf2^{CKO}$ optic cups during OF closure. Phospho-histone H3-labeling to detect proliferating cells in G2/M of the cell cycle revealed an upward trend in the ventral $Nf2^{CKO}$ optic cup that was not significant (Fig. 4A–C; E11.5; $n = 3$). However, we observed a small but significant increase of phospho-histone H3-labeled cells in the ventral quadrant that includes the OF region (Fig. 4D). Since the number of G2/M cells, particularly in the RPE, was generally very low in the optic cup, we additionally analyzed EdU incorporation (Fig. 4E–J). We determined changes in proliferation specifically during the initial alignment of the OF margins, a critical stage for the subsequent attachment and fusion processes during OF closure (E11.0; $n = 4$). The percentage of EdU-labeled cells is significantly increased by 46% in the $Nf2^{CKO}$ RPE (Fig. 4F and G). In contrast, no significant change is detectable in the retina (Fig. 4G and H). The RPE-specific increase in EdU-labeled cell number is specific for the ventral portion in $Nf2^{CKO}$ optic cups, by 79% (Fig. 4F and I; V1–V3), while the dorsal RPE shows no significant change at this stage (Fig. 4F and I). Significantly higher numbers of EdU-labeled RPE cells are observed in all subdivisions of the ventral optic cup, including the OF region (V2; Fig. 4J). Consistent with stimulated proliferation, the total number of cells in the ventral optic cup is significantly expanded in $Nf2^{CKO}$ RPE (Supplementary Material, Figure S3E). In summary, our data indicate that Nf2 disruption in the optic vesicle results in abnormally increased RPE proliferation in the ventral optic cup early in the process of OF closure.

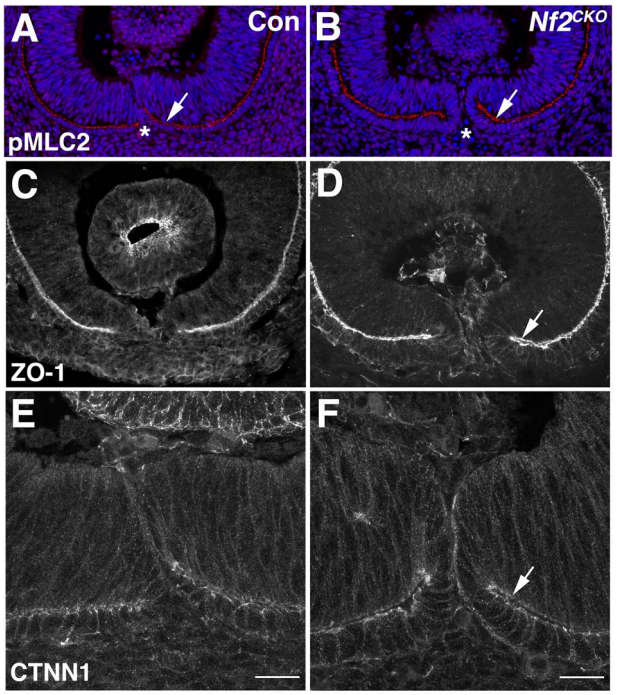

Figure 3. Apicobasal polarity and intercellular junction assembly are maintained during OF closure in the ventral optic cup in *Nf2*^{CKO} embryos. (**A**, **B**, **E**, **F**: E11.5; **C**, **D**: E11.0) A, B: Localization of pMLC2 on the apical surface of the RPE layer appears normal in *Nf2*^{CKO} embryos (B; arrow). Asterisk marks the overlying OF. C, D: Apical distribution of the tight junction component ZO-1 is not affected in the *Nf2*^{CKO} ventral optic cup (D; arrow). The cadherin associated protein α-catenin shows normal localization in the OF and apical space between retina and RPE in *Nf2*^{CKO} eyes (F, arrows). Sagittal view with nasal orientation to the left. Scale bars: 20 µm in E, F.

Ectopic RPE cell number in the dorsal optic cup of *Nf2*^{CKO} embryos

As described above, we detected no significant increase in the percentage of EdU incorporation in the dorsal *Nf2*^{CKO} RPE (Fig. 4I). However, we observed supernumerary cells and frequent cellular crowding in the MITF-labeled RPE layer of the dorsal optic cup (Fig. 5B). Quantification of total cell number revealed a robust significant increase by 47% specifically in the dorsal *Nf2*^{CKO} RPE layer (Fig. 5C; $n = 4$). In contrast, total cell number in the dorsal retina did not change (Fig. 5D). Furthermore, we observed regions with irregular F-actin organization and mis-localization of pMLC2 in the dorsal RPE layer (Fig. 5F and H; arrowheads). Abnormally increased number of RPE cells with disorganization of the RPE layer was maintained later at E13.5, using OTX2 as a marker for differentiating RPE cells (Fig. 5J; arrowheads). Collectively, our data indicate that ocular *Nf2* disruption leads to a significant increase of cell number in the dorsal and ventral RPE layer of the optic cup. This occurs with concomitant acquisition of RPE cell fate and mis-localization of F-Actin and pMLC2. However, size of the *Nf2*^{CKO} eye is unchanged, since measurement of the ocular diameter in embryos did not reveal a significant difference (Supplementary Material, Fig. S3F).

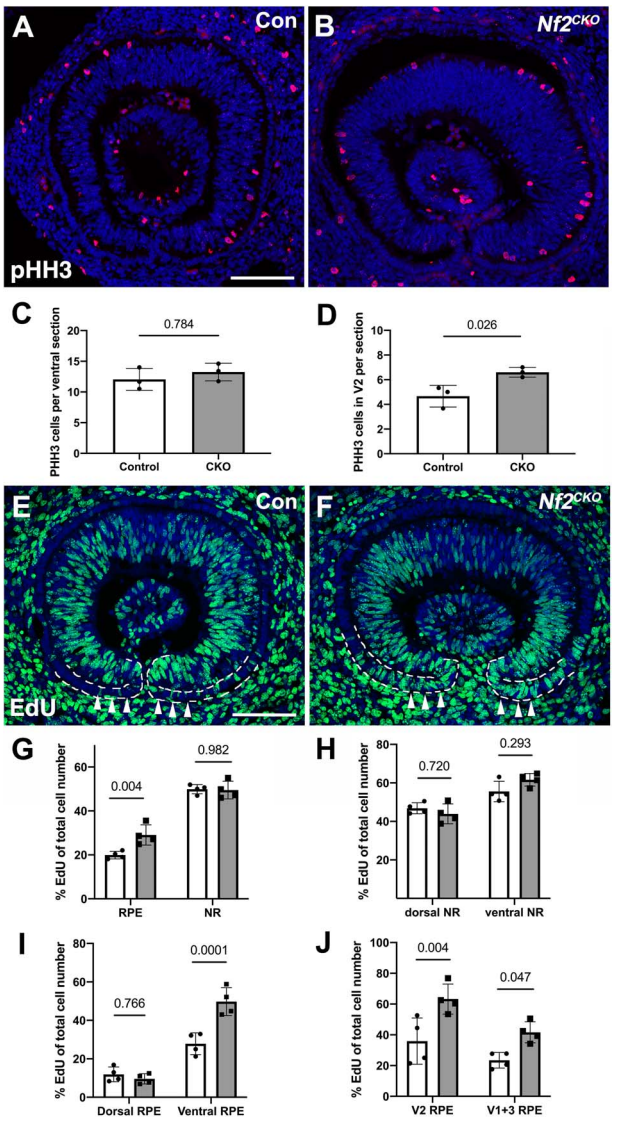

Figure 4. Proliferation is upregulated in the RPE layer in the *Nf2*^{CKO} optic cup. (**A–D**: E11.5; **E–J**: E11.0) A, B: Phospho-histone H3 (pHH3) labeling (red) of control (A) and *Nf2*^{CKO} (B) detects ocular cells in G2/M phases of the cell cycle (red). Dapi is used as a nuclear label (blue). Quantification shows that the number of phospho-histone H3-labeled cells is not changed in the ventral optic cup in *Nf2*^{CKO} eyes (C); however, there is a small significant increase in the ventral-most area that harbors the OF (V2; D). E-J: EdU labeling and quantification. EdU-labeled cells in control (E; green), with nuclear Dapi co-labeling (blue). In the RPE of the *Nf2*^{CKO} ventral optic cup, the number of EdU-labeled cells is increased (F; arrowheads), in comparison with controls (E, arrowheads). Quantitative analysis of EdU incorporation reveals that the number of cells in S-phase is significantly upregulated specifically in the RPE but not in the retina (G, H). (RPE: control: 19.91% ± 1.74 SD; *Nf2*^{CKO}: 29.07% ± 4.60 SD) The increase in EdU-labeled cell number is significant for the ventral RPE (I; control: 27.82% ± 5.66 SD; *Nf2*^{CKO}: 49.86% ± 7.10 SD), while the dorsal RPE shows no change. Significant stimulation of proliferation in the ventral RPE applies to all regions in the ventral optic cup, including the V2 region harboring the OF (J). Data are shown as means ± SD, and *P*-values are indicated above the horizontal lines in each graph (significant < 0.05). Statistical analysis was performed using unpaired, two-tailed Student *T*-test or 2-way analysis of variance (ANOVA) with Sidak's multiple comparison. Images show sagittal view with nasal orientation to the left. Scale bar: 100 µm in A, E.

Alignment and cellular height are altered in the OF margins of the *Nf2*^{CKO} optic cup

Early in the process of OF closure in controls, the fissure margins become tightly aligned, shaped with a convex surface toward the basal space (Fig. 6A). In the *Nf2*^{CKO} OF, the shape of the basal surface of the OF margins is convex, similar to controls, however, alignment of the margins is less advanced (Fig. 6B). At E11.5, margins in control embryos are well aligned along most

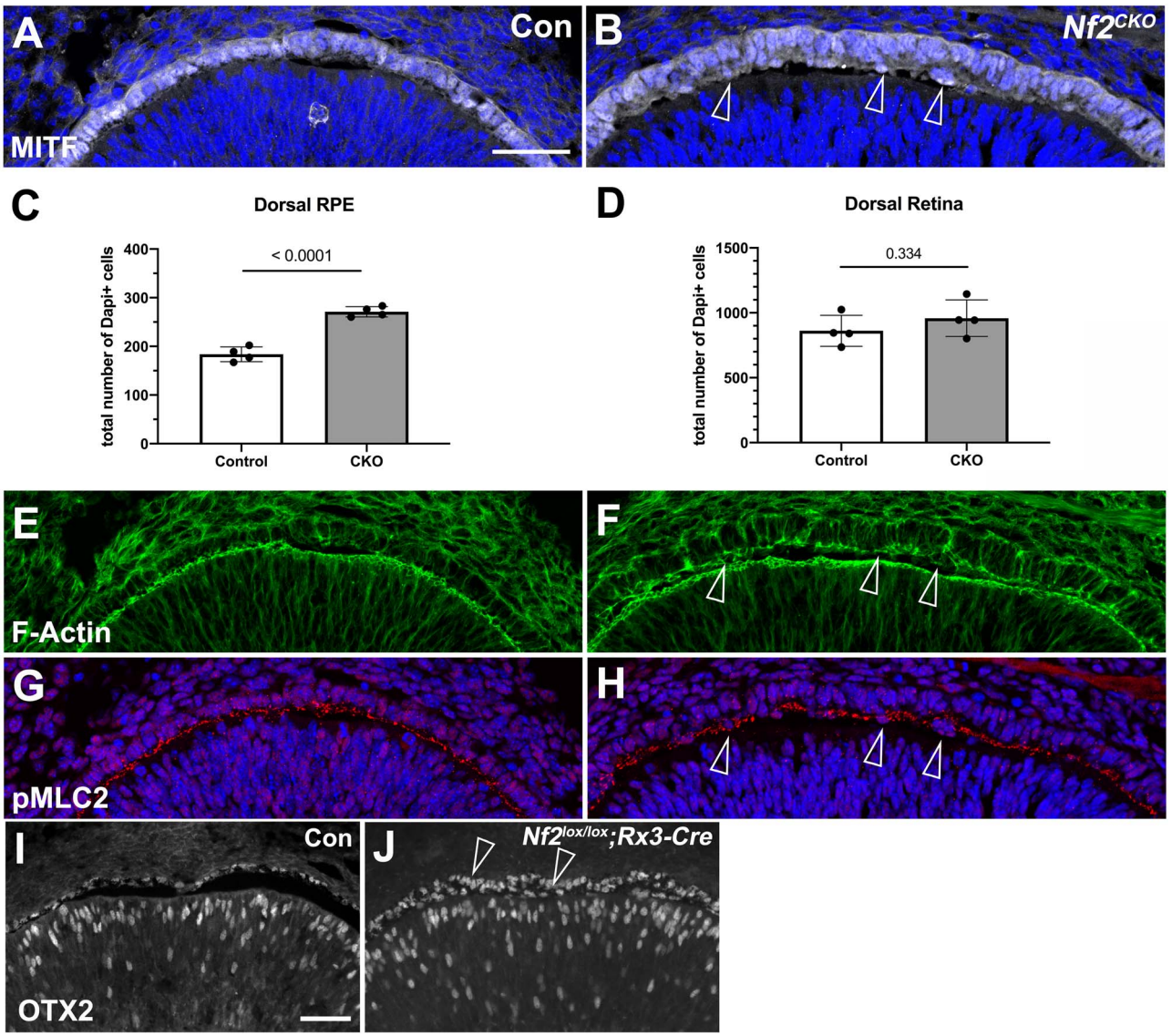

Figure 5. Cell number in the RPE layer is increased in the $Nf2^{CKO}$ dorsal optic cup at E11.0. (**A**, **B**) MITF labeling reveals increased RPE layer thickness in $Nf2^{CKO}$ (B; arrowheads point to ectopic RPE cells located apically). (**C**, **D**) Quantification indicates a significant increase in total cell number in the dorsal RPE in $Nf2^{CKO}$ (C; see Supplementary Material, Figure S3C for subdivisions; control: 183.75 ± 15.13 SD; $Nf2^{CKO}$: 271.00 ± 10.42 SD), while cell number is unchanged in the dorsal retina (D). Data are means ± SD, Student's *T*-test was applied for statistical analysis, and *P*-values are indicated on the horizontal lines in each graph (significance < 0.05). (**E**) Phalloidin labeling in control demonstrates regular organization. (**F**) Phalloidin-labeling $Nf2^{CKO}$ reveals irregularities in localization in the dorsal RPE layer (arrowheads). (**G**) Normal localization of pMLC2 in control dorsal RPE. (**H**) In addition, mis-localization of pMLC2 is detectable in the dorsal RPE layer in $Nf2^{CKO}$ optic cups (arrowheads). (**I**, **J**) OTX2 labeling shows that supernumerary cells persist in the dorsal optic cup at E13.5 (J; arrowheads). Scale bars: 50 μm in A, I.

of the OF with a flattened basal surface (Fig. 6C). In E11.5 $Nf2^{CKO}$ optic cups, we noticed that the shape of the approaching OF margins is consistently altered; the margins maintain a convex shape and the actual extent of contact area between both OF margins is often reduced (Fig. 6D). We quantified this by measuring the extent by which the margins become tightly apposed and determined that the OF in $Nf2^{CKO}$ eyes shows a significant reduction (Fig. 6E).

We observed a tighter cellular packing and crowding with occasional formation of a double layer in $Nf2^{CKO}$ RPE (Fig. 4F). This is most likely caused by increased proliferation particularly in the ventral RPE layer that is continuous with the ventral OF margins (V2; Fig. 4J). In addition, we found that the ventral marginal OF layers appears increased in height along the apicobasal axis and columnar in shape, in comparison with the rather cuboidal organization in controls (Fig. 6C and D; brackets). We measured the apicobasal height of cells lining each temporal and nasal margin in the ventral OF (Supplementary Material, Fig. S3G) and observed a significant increase in cellular height particularly in the temporal OF in $Nf2^{CKO}$ (Fig. 6F). In the nasal OF, cell height measurement showed an upward trend that is not significant (Supplementary Material, Fig. S3H). These results suggest that, in the absence of *Nf2* function, convex shape of the OF margins is maintained, combined with a columnar organization, resulting in insufficient alignment and subsequent failure to fuse.

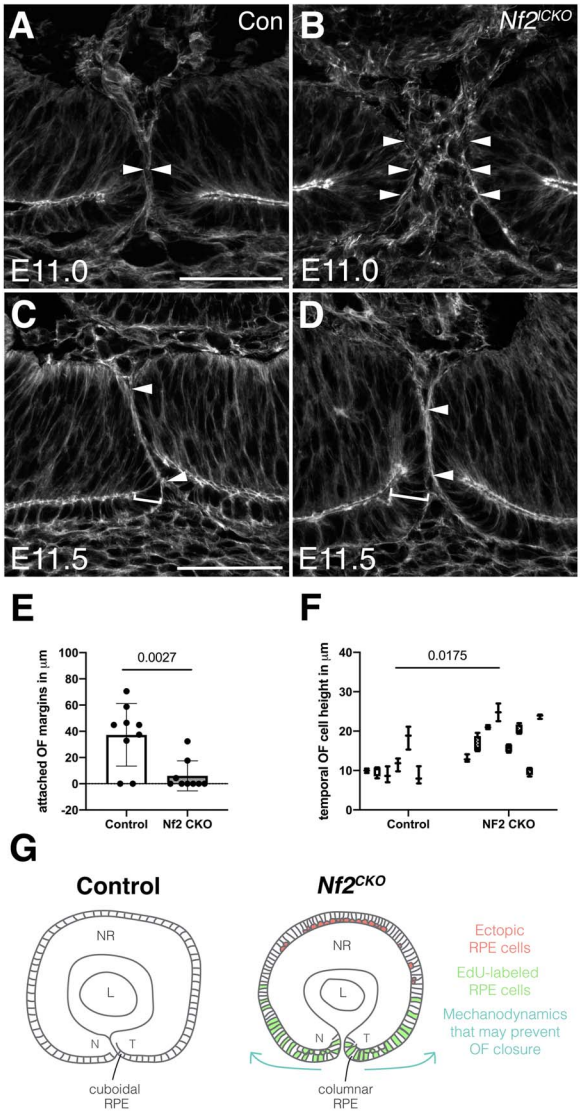

Figure 6. *Rx3-Cre*-mediated disruption of Nf2 results in defective alignment of OF margins during the closure process. (**A–D**) F-actin localization in the OF at E11.0 (A, B) and at E11.5 (C, D) in control (A, C) and $Nf2^{CKO}$ optic cups (B, D). A: In E11.0 control embryos, the OF margins become tightly aligned, shaped with a convex surface toward the basal space (arrowheads). (B) In the $Nf2^{CKO}$ OF, shape of the basal surface of the OF margins is convex, similar to controls, however, alignment of the margins is less advanced (B, arrowheads). At E11.5, the OF margins in controls are well aligned along most of the OF with flattened basal surfaces (C, arrowheads). The RPE layer consists of cuboidal cells (bracket). (D) In $Nf2^{CKO}$ eyes, the OF margins align only partially (arrowheads), exhibit convex shape, and OF cells continuous with the RPE layer show increased height in the apicobasal axis, thereby appearing columnar (bracket). (**E**) Quantification of aligned OF margins. Extent of attached margins was measured in the OF, as outlined in representative examples shown in C, D for aligned OF between arrowheads. In $Nf2^{CKO}$, few margins show close alignment, which is often much reduced, compared with controls (lack of alignment defined = 0). Data are means ± SD and Student's *T*-test was applied for statistical analysis. (**F**) Analysis of cellular height along the apicobasal axis of cells lining the ventral OF margins (see brackets in C, D; Supplementary Material, Figure S3G) reveals significantly increased cellular height in the temporal OF margin. Statistical analysis was performed using nested *T*-test, data are means (with minimal and maximal points). *P*-values are indicated on the horizontal lines in each graph , significance < 0.05 (E, F). (**G**) Proposed model summarizing our observations, for explanation, see text (left: control optic cup; right: $Nf2^{CKO}$). The arrows point to potential effects of RPE hyperproliferation on the mechanodynamics of optic cup growth and apposition of OF margins. Sagittal view with nasal orientation to the left. (NR: neural retina, L: lens, N: nasal, T: temporal). Scale bars: 50 µm in A, C.

Discussion

In summary, our results demonstrate that conditional, ocular disruption of the *Nf2* gene at the optic vesicle stage results in a fully penetrant, distally persistent late-stage defect in OF closure in the mouse embryo (see Fig. 6G for a proposed summary). $Nf2^{CKO}$ eyes show increased nuclear localization of YAP protein in ocular tissues, without apparent defects in formation of junctional complexes or apicobasal polarity in the ventral optic cup. Here, we identify expansion specifically of the RPE layer as a unique underlying cause for coloboma. In $Nf2^{CKO}$ mutant eyes, more cells in the RPE layer in the ventral optic cup, including in the OF margins, proliferate and acquire RPE fate. In the OF margins, cells extend in height or double up as a second layer, and the RPE layer maintains columnar organization instead of transitioning into cells of cuboidal shape. In addition, in the RPE of the dorsal optic cup, *Nf2* loss of function leads to a robust increase in cell number, with local disorganization of the cytoskeleton components F-actin and pMLC2. We propose that this specific effect on proliferation in the RPE layer in the $Nf2^{CKO}$ optic cup may result in changes in mechanodynamics within the growing optic cup, causing the OF margins to align insufficiently.

Nf2 is required for balancing RPE cell number during OF closure

During optic cup morphogenesis, the RPE is required for growth and OF closure; extreme, broad removal of RPE by diphtheria toxin in the early optic cup causes microphthalmia and coloboma (29,107). Growth of the RPE during eye development is dynamic; proliferation is high in the entire optic vesicle (50–60%) and decreases in the RPE substantially soon after invagination (12–25%) (108–111). During normal OF closure, cell number in the mammalian optic cup is tightly balanced by cell proliferation and programmed cell death (13,44,106). Particularly close to the approaching OF margins, proliferation is lower compared with other regions of the optic cup, and deregulated proliferation leads to coloboma (44). This is assumed to prevent cellular crowding in the fissure to allow for cellular reorganization. However, it is unclear from these studies whether cell number specifically in the RPE layer is critical for OF closure (44,91,106). $Nf2^{CKO}$ eyes exhibit a substantial increase in proliferation in the ventral RPE when the OF margins are approaching (by 79%; Fig. 4I), as well as a robust increase of overall cell number in the dorsal RPE. Furthermore, RPE cell expansion is only observed when *Nf2* loss occurs in the optic vesicle and early optic cup, but not at later time points (59) (SR and SF; unpublished observations). This is consistent with the inability of the RPE to renew itself, once differentiation and further maturation commences (112). Few factors have been identified that can promote proliferation and expansion of RPE; these include transgenic hyperactivation of Notch signaling, resulting in microphthalmia and coloboma (29,113), or loss of factors that normally limit proliferation in the developing RPE, such as the cyclin-dependent kinase inhibitor p27Kip1 or DAPL1 (114–116). Collectively, our analysis reveals a unique role for *Nf2* in regulating closure of the OF by restricting RPE proliferation in the optic cup.

Ectopic cells in the outer layer of the $Nf2^{CKO}$ optic cup acquire RPE fate

In the growing optic cup, the presumptive RPE slowly proliferates to maintain a single layer and differentiates into pigmented cells in a central to peripheral and dorsal to ventral gradient,

which is tightly coordinated with growth of the neural retina (88,110,111). Abnormal increases in proliferation in the presumptive RPE in the early optic cup is usually induced by loss of RPE key regulatory gene function or by direct misexpression of factors stimulating proliferation, for example, by modulation of extracellular matrix molecules, extracellular signaling pathways (e.g. FGF, Wnt, Shh), overexpression of oncogenes and loss of key RPE determination genes (112,117). Since the presumptive RPE is bipotential at the early optic cup stage, these manipulations result in transdifferentiation of RPE into retina, with concomitant acquisition of neural retina-specific cell fate and formation of an ectopic retina (for review, see 112). Our findings are unusual; in $Nf2^{CKO}$ eyes, proliferation of the presumptive RPE is strongly upregulated without inducing transdifferentiation into retina, and more RPE cells are produced. This effect is associated with an increase in nuclear YAP localization, consistent with YAP/TAZ's role in regulating RPE cell fate and differentiation in zebrafish and mouse (59,66–68). In addition, YAP mutant eyes develop coloboma in zebrafish. Thus, YAP/TAZ likely exerts a dual role in promoting proliferation and differentiation in the presumptive RPE layer in $Nf2^{CKO}$ optic cups. In premigratory neural crest progenitors, YAP cooperates with PAX3 to transactivate *Mitf*, thus, YAP/TAZ may directly regulate RPE-specific gene expression (92). To further confirm that YAP/TAZ are required for RPE expansion in $Nf2^{CKO}$ embryos, we attempted to block YAP/TEAD interaction by administering Verteporfin; however, this was not successful, possibly due to solubility issues. A recent analysis in mouse revealed that NF2 coordinates later proliferation and differentiation of peripheral retina, ciliary body/iris and RPE by limiting nuclear YAP/TAZ activation (59). Thus, it is very likely that RPE expansion in $Nf2^{CKO}$ eyes is mediated via nuclear translocation of YAP/TAZ and activation of TEAD.

Coloboma may be due to persistent buckling of the OF margins

In $Nf2^{CKO}$ optic cups apposition of both OF margins is significantly decreased; the margins show a higher degree of bending and do not flatten as observed in controls during OF alignment (Fig. 6). Although some optic cups can exhibit fusion at varying degrees proximally close to the optic disc, the OF closure defect in $Nf2^{CKO}$ optic cups is always persistent in the distal optic cup at later stages, excluding a simple delay. While we cannot rule out other potential mechanisms (e.g. constraints provided by the extracellular matrix), our results suggest that over-proliferation in $Nf2^{CKO}$ RPE is likely to be the primary defect. Expanded proliferation may exert a critical mechanical force for promoting tissue buckling, thereby possibly resulting in prolonged convex bending of the OF margins. In a potentially similar scenario, experimentally induced, localized increases in proliferation due to constitutively activated β-catenin can exert mechanical forces to stimulate cortical folding in the embryonic mouse telencephalon (118). Thus, it is possible that similar effects occur on mechanodynamics in the $Nf2^{CKO}$ optic cup.

Our observations suggest that shape and organization of the RPE layer may be important for OF closure. RPE morphogenesis during formation of the optic cup is dynamic; RPE cells transition from a pseudostratified columnar epithelium into a single layer of cuboidal cells (for reviews, see 87,88). Interestingly, in zebrafish, RPE cells flatten further and expand around the retina in the optic cup, independent of cell proliferation and possibly by recruitment of additional cells into the layer (46,119) (for review, see 120). Electron microscopic studies in mouse and hamster suggest that marginal OF cells in the immediate vicinity of the first fusion contact re-orient their polarity during degradation of the basement membrane (9,10). This is supported by live imaging studies in zebrafish, revealing extensive movements and incorporation of OF marginal cells into retina as well as RPE during closure (34,49). In $Nf2^{CKO}$ RPE, cells in the temporal OF margin do not properly transition to a cuboidal monolayer at the time of closure (Fig. 6F). It is possible that the expansion of $Nf2^{CKO}$ RPE results in cellular packing/crowding, preventing cells from re-orienting properly in the OF. This re-arrangement may be necessary to prepare for fusion at the right time. However, we cannot fully exclude that the cells lining the OF harbor a primary intrinsic defect that ultimately prevents proper dissolution of the basement membrane.

Role of Hippo signaling in OF closure in humans

Hippo pathway components have been recently identified as genes with clinical relevance for coloboma (23,53,54,64). Heterozygous loss of function mutations in YAP1 were identified in two unrelated families exhibiting coloboma (3). According to previous studies using animal models, YAP1 may be important for regulating RPE cell fate and RPE proliferation during OF closure in humans (67,68). However, YAP1 is also present in the periocular mesenchyme (Fig. 1; 54), which could be of importance for studies addressing the syndromic occurrence of coloboma. Furthermore, a mutation in the *Tead1* gene causes SCRA, preventing it from interacting with YAP1 (64,121). SCRA manifests as bilateral stripes of atrophic retina and choroid; however, the contribution of RPE defects in disease pathology is not well understood. The protocadherin FAT1 represents a potential upstream regulator of the Hippo pathway, and it is expressed in the RPE (23). A new clinical syndrome with frequent ocular manifestations, in particular coloboma, is reportedly caused by frameshift mutations in the *FAT1* gene that may restrict nuclear localization of YAP. While FAT1 may be critical for cell–cell contact during OF closure, a direct effect on YAP localization was not observed (23). Furthermore, *NF2* mutations cause a variety of ocular defects particularly in the RPE; for example, increased pigmentation and combined retinal and RPE hamartomas (53,122). Importantly, coloboma was observed in NF2 patients with germline nonsense mutations (53). Thus, it is possible that hyperproliferation of the RPE represents an underlying mechanistic cause for some of the observed ocular abnormalities, including coloboma, in individuals with inherited *NF2* mutations.

Material and Methods

Mice

Animal procedures were approved by the Vanderbilt University Medical Center Institutional and Animal Care and Use Committee. $Nf2^{lox/lox}$ mice (77) were crossed with *Rx3-Cre* (80), $Axin2^{lacZ}$ (Jax strain #009120; 98), and $Mitf^{Mi}$ (Jax strain #001573; 123,124). Mouse lines were maintained in a mixed genetic C57BL/6 and CD-1 background. No ocular or extraocular defects were detected in $Nf2^{lox/+}$;*Rx3-Cre* eyes, and littermates without *Cre* allele were used as controls. Some samples were heterozygous for the $Axin2^{lacZ}$ reporter allele, which did not reveal any difference to samples harboring the $Axin2^{wt}$ allele. Some control samples were heterozygous for the *Rd8* mutation, and no difference to *Rd8* wildtype controls was observed. The *Rd8* mutation results from a mutation in the gene *Crb1* (125,126), however, only ocular abnormalities at postnatal ages such as retinal disorganization and photoreceptor degeneration have been observed (127). For

Table 1. Antibodies used in this study

	Dilution	Supplier, Product Number
Primary antibodies		
α-Catenin	1:2000	Sigma; St. Louis, MO; #C2081
β-Galactosidase	1:5000	Cappel; MP Biomedicals, Aurora, OH; #55976
CCND1	1:600	Abcam; Cambridge MA, USA; #16663
Phospho-histone H3	1:1000	EMD Millipore; Billerica, MA; #06-570
Laminin	1:2000	Abcam, Cambridge MA, USA; #ab30320
LEF1	1:125	Cell Signaling; Danvers, MA; #2230
MITF	1:800	Exalpha; Shirley, MA; # X1405M
OTX2	1:1500	EMD Millipore;Temecula; #AB9566
OTX2	1:700	R&D Systems; Minneapolis, MN; #AF1979
PAX2	1:800	BioLegend; San Diego, CA; #901001
PAX6	1:500	BioLegend; San Diego, CA; #901301
Phospho-Myosin Light Chain 2	1:80	Cell Signaling; Danvers, MA; #3674
TBX5	1:200	Novus Biologicals; Centennial, CO; NBP183237
VSX2	1:800	Exalpha; Shirley, MA; #X1180P
YAP1	1:100	Cell Signaling, Danvers; MA; #14074
ZO1	1:100	Thermo Fisher Scientific; Walham, MA; #40-2200
WGA-555	1:200	Thermo Fisher Scientific; Walham, MA; #W32464
Secondary antibodies		
Donkey anti-mouse Alexa Fluor® 594	1:1000	Jackson ImmunoResearch; West Grove, PA; #715-585-150
Donkey anti-mouse Alexa Fluor647	1:800	Thermo Fisher Scientific; Walham, MA; #A31571
Goat anti-mouse Alexa Fluor647	1:1000	Thermo Fisher Scientific; Walham, MA; #A32728
Donkey anti-rabbit Alexa Fluor® 488	1:1000	Jackson ImmunoResearch; West Grove, PA; #711-545-152
Donkey anti-rabbit Alexa Fluor® 594	1:1000	Jackson ImmunoResearch; West Grove, PA; #711-585-152
Goat anti-rabbit Alexa Fluor568	1:1000	Thermo Fisher Scientific; Walham, MA; #A11036
Donkey anti-goat Alexa Fluor568	1:800	Thermo Fisher Scientific; Walham, MA; #A110357
Donkey anti-goat TRITC	1:800	Jackson ImmunoResearch; West Grove, PA; #705-025-147
Donkey anti-sheep Cy™3	1:800	Jackson ImmunoResearch; West Grove, PA; #713-165-003

timed pregnancies, counting started at day 0.5 when the vaginal plug was detected. Embryonic tissues were genotyped using the following primer combinations (19,77,79). The *Nf2* primers CTT CCC AGA CAA GCA GGG TTC (forward, P4) and GAA GGC AGC TTC CTT AAG TC (reverse, P5) generate amplicons for *wt* (305 bp) and *lox* (442 bp); *Rx3-Cre* primers: GTT GGG AGA ATG CTC CGT AA (forward) and GTA TCC CAC AAT TCC TTG CG (reverse) produce a 362 bp amplicon; and the *Axin2*^{lacZ} primers: AAG CTG CGTCGG ATA CTT GAG A (Cs), AGT CCA TCT TCA TTC CGC CTA GC (Cwt), TGG TAA TGC TGC AGT GGC TTG (ClacZ) generate the *Axin*^{wt} (493 bp) and *Axin*^{lacZ} amplicons (400 bp). For genotyping of the *Mitf*^{Mi} allele, tissue samples were processed and genotyped by Transnetyx (Cordova, TN) using Taqman with custom-designed primers: CCTTTCCCATGCTCTTTTCTTGAAG (forward), CTAGCTCCTTAATGCGGTCGTTTAT (reverse), and the following reporter probes to detect the 3-nucleotide mutation: ACGAAGAAGAAGATTTAAC (wildtype allele), AACGAAGAA-GATTTAAC (*Mitf*^{Mi} allele). To detect proliferating cells in S-phase of the cell cycle, pregnant dams received intraperitoneal EdU injections of 30 µg/g body weight 2 h before sacrificing (Thermofisher/Invitrogen, Rockford, IL; #E10187).

Immunohistochemistry

Embryos at the indicated ages were processed as previously described (79). Briefly, embryonic heads were fixed in 4% paraformaldehyde (PFA) for 1 h, cryoprotected in sucrose, sectioned on a Leica CM1950 cryostat at 12 µm and stored at −80°C until further use. For immunohistochemical analysis, sections were processed using antigen retrieval with triton X-100 (0.1%, 1%) and hot citrate buffer pH 6.0. Primary and secondary antibody information is provided in Table 1. Filamentous actin was detected using phalloidin (1:50; Thermo Fisher Scientific, Walham, MA; #A12379). Labeling with WGA-555 (1:200; Thermo Fisher Scientific, Walham, MA; #W32464) was performed prior to antigen retrieval. For detection of apoptotic cells, ApopTag Fluorescein In Situ Apoptosis Detection Kit (EMD Millipore, #S7110) was used according to the manufacturer's instructions. EdU detection was performed using the Click-iT® EdU Imaging Kit (Thermo Fisher Scientific, Walham, MA; #C10637). Sections were counter-labeled with DAPI (Thermo Fisher Scientific, Walham, MA; #D3571) and mounted in Prolong Gold Antifade. A minimum of three eyes from three different embryos from at least two individual litters were analyzed per genotype, time point and marker.

Embryo and whole eye images were captured using an Olympus SZX12 stereomicroscope, equipped with the Olympus MicroFire digital microscope camera U-CMAD3. Epifluorescence images were captured using an upright Olympus BX51 microscope (Tokyo, Japan), mounted with an Olympus XM10 camera. For confocal imaging, the ZEISS LSM 880 and 710 systems were used. Images were processed using Fiji (NIH), Adobe Illustrator 2020 and Adobe Photoshop CS6 and 2020 software.

Quantification analyses

For quantification of CCND1-labeled cells, TUNEL, PHH3-labeling and EdU incorporation, labeled cells were counted in cryostat sections midway through the optic cup (see Supplementary Material, Fig. S1A for sagittal section scheme). The optic cup

was sub-divided into six regions of interest (see Supplementary Material, Fig. S3C) allowing comparison of dorsal and ventral individual subdivisions (D1, D2, D3 and V1, V2, V3) as well as combined data subdivisions to generate values for dorsal (D1–D3) and ventral optic cup domains (V1–V3). The percentage of cells was calculated by determining the number of total cells using DAPI-labeled nuclei. Cell diameter measurements were performed on whole eye images (examples are shown in Fig. 1C and D) by drawing a horizontal line across the center of the eye globe, measured using Fiji software (NIH). We analyzed a minimum of six eyes per genotype from $n = 6$ embryos (five independent litters). To calculate the extent of attachment between OF margins, sagittal cryostat sections labeled with Phalloidin were analyzed. Attachment was defined for tightly apposed OF margins enclosing an area with phalloidin labeling apparent mostly as a single border between the OF margins (for examples, see Figs 3A and 6C, D; Supplementary Material, Fig. S3F). No attachment (set as "0") was defined as a distinguishable gap between the two opposing phalloidin-labeled OF margins, with detectable mesenchymal cells present in the OF (for example, see Fig. 3B). Attachment of OF margins was measured by drawing a straight vertical line, analyzed using Fiji software. We analyzed nine eyes; $n = 7$ embryos from three independent litters. Cellular height was calculated using Phalloidin-labeled images and Fiji software. Specifically, a straight line was applied along the apicobasal extent of each cell (Supplementary Material, Fig. S3F), and 2–4 cells for each temporal or nasal margin of the OF was measured for each sample. At least six eyes from five embryos per genotype, from a minimum of three independent litters were analyzed. Statistical analysis was performed using Prism version 8 (Graphpad, San Diego, CA) for two-way ANOVA with Sidak's multiple comparison or Student's *T*-test. Differences were only considered significant when $P < 0.05$.

To quantify nuclear fluorescence intensity, YAP1 immunofluorescence confocal images of E11.5 cryosections midway through the optic cup were taken at 63× magnification. Two images were taken on either side of the OF in the ventral region of the eye for both $Nf2^{CKO}$ and control tissue. At least 42 nuclei in the RPE and at least 194 nuclei in RPE + retina combined were analyzed per eye. Three control eyes and four $Nf2^{CKO}$ eyes from different embryos were quantified. FIJI software was used to quantify mean nuclear YAP intensity. For quantification, we selected one slice of the *z*-stack (0.5 µm thickness) that was in the center of the nuclear plane of the optic cup. Background was subtracted using the FIJI rolling ball method. Nuclei in the ventral RPE and retina were manually traced using DAPI-counterstained images and added to the region of interest (ROI) manager. The nuclear ROI traces were then overlaid on their respective YAP1 channel to measure the area, mean intensity and integrated density of the ROIs. For statistical analysis, average ROI (nuclei) area and average YAP1 integrated density per nuclei were used and unpaired two-tailed Welch's *t*-tests were performed.

Supplementary Material

Supplementary Material is available at *HMG* online.

Acknowledgements

The authors thank Katrina Hofstetter and Burns Newsome for technical support and Marco Giovannini, Ed Levine and members of the Levine and Fuhrmann laboratories as well as Jenny C. Schafer for helpful comments. We thank Jin Woo Kim for sharing data, Edward Levine for providing the $Mitf^{Mi}$ allele and Marco Giovannini for providing the conditional Nf2 allele.

Conflict of Interest statement. None declared.

Funding

National Institutes of Health (R01 EY024373 to S.F., T32 HD007502 Training Grant in Stem Cell and Regenerative Developmental Biology to S.R., Core Grant P30 EY008126); a Catalyst Award to S.F. from Research to Prevent Blindness Inc./American Macular Degeneration Foundation, an unrestricted award to the Department of Ophthalmology and Visual Sciences from Research to Prevent Blindness, Inc.; the Vanderbilt University Medical Center Cell Imaging Shared Resource Core Facility (Clinical and Translational Science Award Grant UL1 RR024975 from National Center for Research Resources).

References

1. Morrison, D., Fitz Patrick, D., Hanson, I., Williamson, K., van Heyningen, V., Fleck, B., Jones, I., Chalmers, J. and Campbell, H. (2002) National study of microphthalmia, anophthalmia, and coloboma (MAC) in Scotland: investigation of genetic aetiology. *J. Med. Genet.*, **39**, 16–22.
2. Clementi, M., Turolla, L., Mammi, I. and Tenconi, R. (1992) Clinical anophthalmia: an epidemiological study in Northeast Italy based on 368,256 consecutive births. *Teratology*, **46**, 551–553.
3. Williamson, K.A. and Fitz Patrick, D.R. (2014) The genetic architecture of microphthalmia, anophthalmia and coloboma. *Eur. J. Med. Genet.*, **57**, 369–380.
4. Shah, S.P., Taylor, A.E., Sowden, J.C., Ragge, N.K., Russell-Eggitt, I., Rahi, J.S., Gilbert, C.E. and Surveillance of Eye Anomalies Special Interest Group (2011) Anophthalmos, microphthalmos, and typical coloboma in the United Kingdom: a prospective study of incidence and risk. *Invest. Ophthalmol. Vis. Sci.*, **52**, 558–564.
5. Maumenee, I.H. and Mitchell, T.N. (1990) Colobomatous malformations of the eye. *Trans. Am. Ophthalmol. Soc.*, **88**, 123–132 discussion 133-125.
6. Chang, L., Blain, D., Bertuzzi, S. and Brooks, B.P. (2006) Uveal coloboma: clinical and basic science update. *Curr. Opin. Ophthalmol.*, **17**, 447–470.
7. George, A., Cogliati, T. and Brooks, B.P. (2020) Genetics of syndromic ocular coloboma: CHARGE and COACH syndromes. *Exp. Eye Res.*, **193**, 107940.
8. AS, A.L., Gregory-Evans, C.Y. and Gregory-Evans, K. (2019) An update on the genetics of ocular coloboma. *Hum. Genet.*, **138**, 865–880.
9. Hero, I. (1990) Optic fissure closure in the normal cinnamon mouse. An ultrastructural study. *Invest. Ophthalmol. Vis. Sci.*, **31**, 197–216.
10. Geeraets, R. (1976) An electron microscopic study of the closure of the optic fissure in the golden hamster. *Am. J. Anat.*, **145**, 411–431.
11. O'Rahilly, R. (1983) The timing and sequence of events in the development of the human eye and ear during the embryonic period proper. *Anat. Embryol.*, **168**, 87–99.
12. Hero, I. (1989) The optic fissure in the normal and microphthalmic mouse. *Exp. Eye Res.*, **49**, 229–239.
13. Patel, A. and Sowden, J.C. (2019) Genes and pathways in optic fissure closure. *Semin. Cell Dev. Biol.*, **91**, 55–65.

14. Reis, L.M. and Semina, E.V. (2015) Conserved genetic pathways associated with microphthalmia, anophthalmia, and coloboma. *Birth Defects Res. C Embryo Today*, **105**, 96–113.
15. Bosze, B., Moon, M.S., Kageyama, R. and Brown, N.L. (2020) Simultaneous requirements for Hes1 in retinal neurogenesis and optic cup-stalk boundary maintenance. *J. Neurosci.*, **40**, 1501–1513.
16. Pillai-Kastoori, L., Wen, W., Wilson, S.G., Strachan, E., Lo-Castro, A., Fichera, M., Musumeci, S.A., Lehmann, O.J. and Morris, A.C. (2014) Sox11 is required to maintain proper levels of hedgehog signaling during vertebrate ocular morphogenesis. *PLoS Genet.*, **10**, e1004491.
17. Wen, W., Pillai-Kastoori, L., Wilson, S.G. and Morris, A.C. (2015) Sox4 regulates choroid fissure closure by limiting hedgehog signaling during ocular morphogenesis. *Dev. Biol.*, **399**, 139–153.
18. George, A., Zand, D.J., Hufnagel, R.B., Sharma, R., Sergeev, Y.V., Legare, J.M., Rice, G.M., Scott Schwoerer, J.A., Rius, M., Tetri, L. *et al.* (2016) Biallelic mutations in MITF cause Coloboma, Osteopetrosis, Microphthalmia, macrocephaly, albinism, and deafness. *Am. J. Hum. Genet.*, **99**, 1388–1394.
19. Alldredge, A. and Fuhrmann, S. (2016) Loss of Axin2 causes ocular defects during mouse eye development. *Invest. Ophthalmol. Vis. Sci.*, **57**, 5253–5262.
20. Gordon, H.B., Lusk, S., Carney, K.R., Wirick, E.O., Murray, B.F. and Kwan, K.M. (2018) Hedgehog signaling regulates cell motility and optic fissure and stalk formation during vertebrate eye morphogenesis. *Development*, **145**, dev165068.
21. Hocking, J.C., Famulski, J.K., Yoon, K.H., Widen, S.A., Bernstein, C.S., Koch, S., Weiss, O., Consortium, F.C., Agarwala, S., Inbal, A. *et al.* (2018) Morphogenetic defects underlie superior Coloboma, a newly identified closure disorder of the dorsal eye. *PLoS Genet.*, **14**, e1007246.
22. Knickmeyer, M.D., Mateo, J.L., Eckert, P., Roussa, E., Rahhal, B., Zuniga, A., Krieglstein, K., Wittbrodt, J. and Heermann, S. (2018) TGFbeta-facilitated optic fissure fusion and the role of bone morphogenetic protein antagonism. *Open Biol.*, **8**, 170134.
23. Lahrouchi, N., George, A., Ratbi, I., Schneider, R., Elalaoui, S.C., Moosa, S., Bharti, S., Sharma, R., Abu-Asab, M., Onojafe, F. *et al.* (2019) Homozygous frameshift mutations in FAT1 cause a syndrome characterized by colobomatous-microphthalmia, ptosis, nephropathy and syndactyly. *Nat. Commun.*, **10**, 1180.
24. Smith, R., Huang, Y.T., Tian, T., Vojtasova, D., Mesalles-Naranjo, O., Pollard, S.M., Pratt, T., Price, D.J. and Fotaki, V. (2017) The transcription factor Foxg1 promotes optic fissure closure in the mouse by suppressing Wnt8b in the nasal optic stalk. *J. Neurosci.*, **37**, 7975–7993.
25. Yan, X., Atorf, J., Ramos, D., Thiele, F., Weber, S., Dalke, C., Sun, M., Puk, O., Michel, D., Fuchs, H. *et al.* (2020) Mutation in Bmpr1b leads to optic disc Coloboma and ventral retinal gliosis in mice. *Invest. Ophthalmol. Vis. Sci.*, **61**, 44.
26. Ceroni, F., Aguilera-Garcia, D., Chassaing, N., Bax, D.A., Blanco-Kelly, F., Ramos, P., Tarilonte, M., Villaverde, C., da Silva, L.R.J., Ballesta-Martinez, M.J. *et al.* (2019) New GJA8 variants and phenotypes highlight its critical role in a broad spectrum of eye anomalies. *Hum. Genet.*, **138**, 1027–1042.
27. Hardy, H., Prendergast, J.G., Patel, A., Dutta, S., Trejo-Reveles, V., Kroeger, H., Yung, A.R., Goodrich, L.V., Brooks, B., Sowden, J.C. *et al.* (2019) Detailed analysis of chick optic fissure closure reveals Netrin-1 as an essential mediator of epithelial fusion. *Elife*, **8**, e43877.
28. Sedykh, I., Yoon, B., Roberson, L., Moskvin, O., Dewey, C.N. and Grinblat, Y. (2017) Zebrafish zic2 controls formation of periocular neural crest and choroid fissure morphogenesis. *Dev. Biol.*, **429**, 92–104.
29. Ha, T., Moon, K.H., Dai, L., Hatakeyama, J., Yoon, K., Park, H.S., Kong, Y.Y., Shimamura, K. and Kim, J.W. (2017) The retinal pigment epithelium is a notch Signaling niche in the mouse retina. *Cell Rep.*, **19**, 351–363.
30. Liu, C., Widen, S.A., Williamson, K.A., Ratnapriya, R., Gerth-Kahlert, C., Rainger, J., Alur, R.P., Strachan, E., Manjunath, S.H., Balakrishnan, A. *et al.* (2016) A secreted WNT-ligand-binding domain of FZD5 generated by a frameshift mutation causes autosomal dominant coloboma. *Hum. Mol. Genet.*, **25**, 1382–1391.
31. Bryan, C.D., Casey, M.A., Pfeiffer, R.L., Jones, B.W. and Kwan, K.M. (2020) Optic cup morphogenesis requires neural crest-mediated basement membrane assembly. *Development*, **147**, dev181420.
32. Bryan, C.D., Chien, C.B. and Kwan, K.M. (2016) Loss of laminin alpha 1 results in multiple structural defects and divergent effects on adhesion during vertebrate optic cup morphogenesis. *Dev. Biol.*, **416**, 324–337.
33. James, A., Lee, C., Williams, A.M., Angileri, K., Lathrop, K.L. and Gross, J.M. (2016) The hyaloid vasculature facilitates basement membrane breakdown during choroid fissure closure in the zebrafish eye. *Dev. Biol.*, **419**, 262–272.
34. Gestri, G., Bazin-Lopez, N., Scholes, C. and Wilson, S.W. (2018) Cell Behaviors during closure of the choroid fissure in the developing eye. *Front. Cell. Neurosci.*, **12**, 42.
35. Carrara, N., Weaver, M., Piedade, W.P., Vocking, O. and Famulski, J.K. (2019) Temporal characterization of optic fissure basement membrane composition suggests nidogen may be an initial target of remodeling. *Dev. Biol.*, **452**, 43–54.
36. Sinagoga, K.L., Larimer-Picciani, A.M., George, S.M., Spencer, S.A., Lister, J.A. and Gross, J.M. (2020) Mitf-family transcription factor function is required within cranial neural crest cells to promote choroid fissure closure. *Development*, **147**, dev187047
37. Rainger, J., Williamson, K.A., Soares, D.C., Truch, J., Kurian, D., Gillessen-Kaesbach, G., Seawright, A., Prendergast, J., Halachev, M., Wheeler, A. *et al.* (2017) A recurrent de novo mutation in ACTG1 causes isolated ocular coloboma. *Hum. Mutat.*, **38**, 942–946.
38. Verloes, A., Di Donato, N., Masliah-Planchon, J., Jongmans, M., Abdul-Raman, O.A., Albrecht, B., Allanson, J., Brunner, H., Bertola, D., Chassaing, N. *et al.* (2015) Baraitser-winter cerebrofrontofacial syndrome: delineation of the spectrum in 42 cases. *Eur. J. Hum. Genet.*, **23**, 292–301.
39. Turner, K.J., Hoyle, J., Valdivia, L.E., Cerveny, K.L., Hart, W., Mangoli, M., Geisler, R., Rees, M., Houart, C., Poole, R.J. *et al.* (2019) Abrogation of stem loop binding protein (Slbp) function leads to a failure of cells to transition from proliferation to differentiation, retinal coloboma and midline axon guidance deficits. *PloS One*, **e0211073**, 14.
40. Cao, M., Ouyang, J., Guo, J., Lin, S. and Chen, S. (2018) Metalloproteinase Adamts16 is required for proper closure of the optic fissure. *Invest. Ophthalmol. Vis. Sci.*, **59**, 1167–1177.
41. Tsuji, N., Matsuura, T., Narama, I., Yoshiki, A. and Ozaki, K. (2018) Macrophage-associated Gelatinase degrades basement membrane at the optic fissure margins during normal ocular development in mice. *Invest. Ophthalmol. Vis. Sci.*, **59**, 1368–1373.

42. Pereira Piedade, W., Veith, S. and Famulski, J.K. (2019) Ubiquitin-mediated proteasome degradation regulates optic fissure fusion. *Biol. Open*, **8**, bio044974.
43. Gath, N. and Gross, J.M. (2019) Zebrafish mab21l2 mutants possess severe defects in optic cup morphogenesis, lens and cornea development. *Dev. Dyn.*, **248**, 514–529.
44. Noh, H., Lee, H., Park, E. and Park, S. (2016) Proper closure of the optic fissure requires ephrin A5-Eph B2-JNK signaling. *Development*, **143**, 461–472.
45. Heermann, S., Schutz, L., Lemke, S., Krieglstein, K. and Wittbrodt, J. (2015) Eye morphogenesis driven by epithelial flow into the optic cup facilitated by modulation of bone morphogenetic protein. *Elife*, **4**, e05216.
46. Kwan, K.M., Otsuna, H., Kidokoro, H., Carney, K.R., Saijoh, Y. and Chien, C.B. (2012) A complex choreography of cell movements shapes the vertebrate eye. *Development*, **139**, 359–372.
47. Picker, A., Cavodeassi, F., Machate, A., Bernauer, S., Hans, S., Abe, G., Kawakami, K., Wilson, S.W. and Brand, M. (2009) Dynamic coupling of pattern formation and morphogenesis in the developing vertebrate retina. *PLoS Biol.*, **7**, e1000214.
48. Bernstein, C.S., Anderson, M.T., Gohel, C., Slater, K., Gross, J.M. and Agarwala, S. (2018) The cellular bases of choroid fissure formation and closure. *Dev. Biol.*, **440**, 137–151.
49. Eckert, P., Knickmeyer, M.D. and Heermann, S. (2020) In vivo analysis of optic fissure fusion in Zebrafish: Pioneer cells, basal lamina, Hyaloid vessels, and how fissure fusion is affected by BMP. *Int. J. Mol. Sci.*, **21**, 2760.
50. Brown, J.D., Dutta, S., Bharti, K., Bonner, R.F., Munson, P.J., Dawid, I.B., Akhtar, A.L., Onojafe, I.F., Alur, R.P., Gross, J.M. *et al.* (2009) Expression profiling during ocular development identifies 2 Nlz genes with a critical role in optic fissure closure. *Proc. Natl. Acad. Sci. USA*, **106**, 1462–1467.
51. Cao, M., Ouyang, J., Liang, H., Guo, J., Lin, S., Yang, S., Xie, T. and Chen, S. (2018) Regional gene expression profile comparison reveals the unique Transcriptome of the optic fissure. *Invest. Ophthalmol. Vis. Sci.*, **59**, 5773–5784.
52. Richardson, R., Owen, N., Toms, M., Young, R.M., Tracey-White, D. and Moosajee, M. (2019) Transcriptome profiling of zebrafish optic fissure fusion. *Sci. Rep.*, **9**, 1541.
53. Chan, C.C., Koch, C.A., Kaiser-Kupfer, M.I., Parry, D.M., Gutmann, D.H., Zhuang, Z. and Vortmeyer, A.O. (2002) Loss of heterozygosity for the NF2 gene in retinal and optic nerve lesions of patients with neurofibromatosis 2. *J. Pathol.*, **198**, 14–20.
54. Williamson, K.A., Rainger, J., Floyd, J.A., Ansari, M., Meynert, A., Aldridge, K.V., Rainger, J.K., Anderson, C.A., Moore, A.T., Hurles, M.E. *et al.* (2014) Heterozygous loss-of-function mutations in YAP1 cause both isolated and syndromic optic fissure closure defects. *Am. J. Hum. Genet.*, **94**, 295–302.
55. Painter, S.L., Sipkova, Z., Emmanouil, B., Halliday, D., Parry, A. and Elston, J.S. (2019) Neurofibromatosis type 2-related eye disease correlated with genetic severity type. *J. Neuroophthalmol.*, **39**, 44–49.
56. Waisberg, V., Rodrigues, L.O.C., Nehemy, M.B., Bastos-Rodrigues, L. and de Miranda, D.M. (2019) Ocular alterations, molecular findings, and three novel pathological mutations in a series of NF2 patients. *Graefes Arch. Clin. Exp. Ophthalmol.*, **257**, 1453–1458.
57. Ragge, N.K., Baser, M.E., Riccardi, V.M. and Falk, R.E. (1997) The ocular presentation of neurofibromatosis 2. *Eye*, **11**, 12–18.
58. McLaughlin, M.E., Kruger, G.M., Slocum, K.L., Crowley, D., Michaud, N.A., Huang, J., Magendantz, M. and Jacks, T. (2007) The Nf2 tumor suppressor regulates cell-cell adhesion during tissue fusion. *Proc. Natl. Acad. Sci. USA*, **104**, 3261–3266.
59. Moon, K.H., Kim, H.T., Lee, D., Rao, M.B., Levine, E.M., Lim, D.S. and Kim, J.W. (2018) Differential expression of NF2 in Neuroepithelial compartments is necessary for mammalian eye development. *Dev. Cell*, **44**, 13–28 e13.
60. Bretscher, A., Edwards, K. and Fehon, R.G. (2002) ERM proteins and merlin: integrators at the cell cortex. *Nat. Rev. Mol. Cell Biol.*, **3**, 586–599.
61. Cooper, J. and Giancotti, F.G. (2014) Molecular insights into NF2/Merlin tumor suppressor function. *FEBS Lett.*, **588**, 2743–2752.
62. Mota, M. and Shevde, L.A. (2020) Merlin regulates signaling events at the nexus of development and cancer. *Cell Commun. Signal*, **18**, 63.
63. Gladden, A.B., Hebert, A.M., Schneeberger, E.E. and McClatchey, A.I. (2010) The NF2 tumor suppressor, Merlin, regulates epidermal development through the establishment of a junctional polarity complex. *Dev. Cell*, **19**, 727–739.
64. Fossdal, R., Jonasson, F., Kristjansdottir, G.T., Kong, A., Stefansson, H., Gosh, S., Gulcher, J.R. and Stefansson, K. (2004) A novel TEAD1 mutation is the causative allele in Sveinsson's chorioretinal atrophy (helicoid peripapillary chorioretinal degeneration). *Hum. Mol. Genet.*, **13**, 975–981.
65. Holt, R., Ceroni, F., Bax, D.A., Broadgate, S., Diaz, D.G., Santos, C., Gerrelli, D. and Ragge, N.K. (2017) New variant and expression studies provide further insight into the genotype-phenotype correlation in YAP1-related developmental eye disorders. *Sci. Rep.*, **7**, 7975.
66. Asaoka, Y., Hata, S., Namae, M., Furutani-Seiki, M. and Nishina, H. (2014) The Hippo pathway controls a switch between retinal progenitor cell proliferation and photoreceptor cell differentiation in zebrafish. *PloS One*, **9**, e97365.
67. Kim, J.Y., Park, R., Lee, J.H., Shin, J., Nickas, J., Kim, S. and Cho, S.H. (2016) Yap is essential for retinal progenitor cell cycle progression and RPE cell fate acquisition in the developing mouse eye. *Dev. Biol.*, **419**, 336–347.
68. Miesfeld, J.B., Gestri, G., Clark, B.S., Flinn, M.A., Poole, R.J., Bader, J.R., Besharse, J.C., Wilson, S.W. and Link, B.A. (2015) Yap and Taz regulate retinal pigment epithelial cell fate. *Development*, **142**, 3021–3032.
69. Neal, S.J., Zhou, Q. and Pignoni, F. (2020) STRIPAK-PP2A regulates Hippo-Yorkie signaling to suppress retinal fate in the drosophila eye disc peripodial epithelium. *J. Cell Sci.*, **133**, jcs237834.
70. Zhang, H., Deo, M., Thompson, R.C., Uhler, M.D. and Turner, D.L. (2012) Negative regulation of yap during neuronal differentiation. *Dev. Biol.*, **361**, 103–115.
71. Zhang, T., Zhou, Q. and Pignoni, F. (2011) Yki/YAP, Sd/TEAD and Hth/MEIS control tissue specification in the drosophila eye disc epithelium. *PloS One*, **6**, e22278.
72. Lee, M., Goraya, N., Kim, S. and Cho, S.H. (2018) Hippo-yap signaling in ocular development and disease. *Dev. Dyn.*, **247**, 794–806.
73. Moon, K.H. and Kim, J.W. (2018) Hippo Signaling circuit and divergent tissue growth in mammalian eye. *Mol. Cells*, **41**, 257–263.
74. Zhu, J.Y., Lin, S. and Ye, J. (2018) YAP and TAZ, the conductors that orchestrate eye development, homeostasis, and disease. *J. Cell. Physiol.*, **234**, 246–258.

75. Huynh, D.P., Tran, T.M., Nechiporuk, T. and Pulst, S.M. (1996) Expression of neurofibromatosis 2 transcript and gene product during mouse fetal development. *Cell Growth Differ.*, **7**, 1551–1561.
76. Wiley, L.A., Dattilo, L.K., Kang, K.B., Giovannini, M. and Beebe, D.C. (2010) The tumor suppressor merlin is required for cell cycle exit, terminal differentiation, and cell polarity in the developing murine lens. *Invest. Ophthalmol. Vis. Sci.*, **51**, 3611–3618.
77. Giovannini, M., Robanus-Maandag, E., van der Valk, M., Niwa-Kawakita, M., Abramowski, V., Goutebroze, L., Woodruff, J.M., Berns, A. and Thomas, G. (2000) Conditional biallelic Nf2 mutation in the mouse promotes manifestations of human neurofibromatosis type 2. *Genes Dev.*, **14**, 1617–1630.
78. McClatchey, A.I., Saotome, I., Ramesh, V., Gusella, J.F. and Jacks, T. (1997) The Nf2 tumor suppressor gene product is essential for extraembryonic development immediately prior to gastrulation. *Genes Dev.*, **11**, 1253–1265.
79. Bankhead, E.J., Colasanto, M.P., Dyorich, K.M., Jamrich, M., Murtaugh, L.C. and Fuhrmann, S. (2015) Multiple requirements of the focal dermal hypoplasia gene porcupine during ocular morphogenesis. *Am. J. Pathol.*, **185**, 197–213.
80. Swindell, E.C., Bailey, T.J., Loosli, F., Liu, C., Amaya-Manzanares, F., Mahon, K.A., Wittbrodt, J. and Jamrich, M. (2006) Rx-Cre, a tool for inactivation of gene expression in the developing retina. *Genesis*, **44**, 361–363.
81. Akhmametyeva, E.M., Mihaylova, M.M., Luo, H., Kharzai, S., Welling, D.B. and Chang, L.S. (2006) Regulation of the neurofibromatosis 2 gene promoter expression during embryonic development. *Dev. Dyn.*, **235**, 2771–2785.
82. Hamon, A., Masson, C., Bitard, J., Gieser, L., Roger, J.E. and Perron, M. (2017) Retinal degeneration triggers the activation of YAP/TEAD in reactive Muller cells. *Invest. Ophthalmol. Vis. Sci.*, **58**, 1941–1953.
83. Miesfeld, J.B. and Link, B.A. (2014) Establishment of transgenic lines to monitor and manipulate yap/Taz-Tead activity in zebrafish reveals both evolutionarily conserved and divergent functions of the Hippo pathway. *Mech. Dev.*, **133**, 177–188.
84. Monroe, T.O., Hill, M.C., Morikawa, Y., Leach, J.P., Heallen, T., Cao, S., Krijger, P.H.L., de Laat, W., Wehrens, X.H.T., Rodney, G.G. *et al.* (2019) YAP partially reprograms chromatin accessibility to directly induce adult cardiogenesis in vivo. *Dev. Cell*, **48**, 765, e767–779.
85. Cardozo, M.J., Almuedo-Castillo, M. and Bovolenta, P. (2020) Patterning the vertebrate retina with morphogenetic signaling pathways. *Neuroscientist*, **26**, 185–196.
86. Martinez-Morales, J.R., Rodrigo, I. and Bovolenta, P. (2004) Eye development: a view from the retina pigmented epithelium. *Bioessays*, **26**, 766–777.
87. Moreno-Marmol, T., Cavodeassi, F. and Bovolenta, P. (2018) Setting eyes on the retinal pigment epithelium. *Front. Cell Dev. Biol.*, **6**, 145.
88. Bharti, K., Nguyen, M.T., Skuntz, S., Bertuzzi, S. and Arnheiter, H. (2006) The other pigment cell: specification and development of the pigmented epithelium of the vertebrate eye. *Pigment Cell Res.*, **19**, 380–394.
89. Bumsted, K.M. and Barnstable, C.J. (2000) Dorsal retinal pigment epithelium differentiates as neural retina in the microphthalmia (mi/mi) mouse. *Invest. Ophthalmol. Vis. Sci.*, **41**, 903–908.
90. Cai, Z., Tao, C., Li, H., Ladher, R., Gotoh, N., Feng, G.S., Wang, F. and Zhang, X. (2013) Deficient FGF signaling causes optic nerve dysgenesis and ocular coloboma. *Development*, **140**, 2711–2723.
91. Chen, S., Li, H., Gaudenz, K., Paulson, A., Guo, F., Trimble, R., Peak, A., Seidel, C., Deng, C., Furuta, Y. *et al.* (2013) Defective FGF signaling causes coloboma formation and disrupts retinal neurogenesis. *Cell Res.*, **23**, 254–273.
92. Manderfield, L.J., Engleka, K.A., Aghajanian, H., Gupta, M., Yang, S., Li, L., Baggs, J.E., Hogenesch, J.B., Olson, E.N. and Epstein, J.A. (2014) Pax3 and Hippo signaling coordinate melanocyte gene expression in neural crest. *Cell Rep.*, **9**, 1885–1895.
93. Fu, X., Sun, H., Klein, W.H. and Mu, X. (2006) Beta-catenin is essential for lamination but not neurogenesis in mouse retinal development. *Dev. Biol.*, **299**, 424–437.
94. Fujimura, N., Taketo, M.M., Mori, M., Korinek, V. and Kozmik, Z. (2009) Spatial and temporal regulation of Wnt/beta-catenin signaling is essential for development of the retinal pigment epithelium. *Dev. Biol.*, **334**, 31–45.
95. Hagglund, A.C., Berghard, A. and Carlsson, L. (2013) Canonical Wnt/beta-catenin signalling is essential for optic cup formation. *PloS One*, **8**, e81158.
96. Westenskow, P., Piccolo, S. and Fuhrmann, S. (2009) Beta-catenin controls differentiation of the retinal pigment epithelium in the mouse optic cup by regulating Mitf and Otx2 expression. *Development*, **136**, 2505–2510.
97. Kim, M., Kim, S., Lee, S.H., Kim, W., Sohn, M.J., Kim, H.S., Kim, J. and Jho, E.H. (2016) Merlin inhibits Wnt/beta-catenin signaling by blocking LRP6 phosphorylation. *Cell Death Differ.*, **23**, 1638–1647.
98. Lustig, B., Jerchow, B., Sachs, M., Weiler, S., Pietsch, T., Karsten, U., van de Wetering, M., Clevers, H., Schlag, P.M., Birchmeier, W. *et al.* (2002) Negative feedback loop of Wnt signaling through upregulation of conductin/axin2 in colorectal and liver tumors. *Mol. Cell Biol.*, **22**, 1184–1193.
99. Porazinski, S., Wang, H., Asaoka, Y., Behrndt, M., Miyamoto, T., Morita, H., Hata, S., Sasaki, T., Krens, S.F.G., Osada, Y. *et al.* (2015) YAP is essential for tissue tension to ensure vertebrate 3D body shape. *Nature*, **521**, 217–221.
100. Eiraku, M., Takata, N., Ishibashi, H., Kawada, M., Sakakura, E., Okuda, S., Sekiguchi, K., Adachi, T. and Sasai, Y. (2011) Self-organizing optic-cup morphogenesis in three-dimensional culture. *Nature*, **472**, 51–56.
101. Cole, L.K. and Ross, L.S. (2001) Apoptosis in the developing zebrafish embryo. *Dev. Biol.*, **240**, 123–142.
102. Lee, J., Lee, B.K. and Gross, J.M. (2013) Bcl6a function is required during optic cup formation to prevent p53-dependent apoptosis and colobomata. *Hum. Mol. Genet.*, **22**, 3568–3582.
103. Bozanic, D., Tafra, R. and Saraga-Babic, M. (2003) Role of apoptosis and mitosis during human eye development. *Eur. J. Cell Biol.*, **82**, 421–429.
104. Laemle, L.K., Puszkarczuk, M. and Feinberg, R.N. (1999) Apoptosis in early ocular morphogenesis in the mouse. *Brain Res. Dev. Brain Res.*, **112**, 129–133.
105. Ozeki, H., Ogura, Y., Hirabayashi, Y. and Shimada, S. (2000) Apoptosis is associated with formation and persistence of the embryonic fissure. *Curr. Eye Res.*, **20**, 367–372.
106. Kim, T.H., Goodman, J., Anderson, K.V. and Niswander, L. (2007) Phactr4 regulates neural tube and optic fissure closure by controlling PP1-, Rb-, and E2F1-regulated cell-cycle progression. *Dev. Cell*, **13**, 87–102.
107. Raymond, S.M. and Jackson, I.J. (1995) The retinal pigmented epithelium is required for development and

maintenance of the mouse neural retina. *Curr. Biol.*, **5**, 1286–1295.
108. Huang, J., Liu, Y., Oltean, A. and Beebe, D.C. (2015) Bmp4 from the optic vesicle specifies murine retina formation. *Dev. Biol.*, **402**, 119–126.
109. Lee, H.Y., Wroblewski, E., Philips, G.T., Stair, C.N., Conley, K., Reedy, M., Mastick, G.S. and Brown, N.L. (2005) Multiple requirements for Hes1 during early eye formation. *Dev. Biol.*, **284**, 464–478.
110. Bodenstein, L. and Sidman, R.L. (1987) Growth and development of the mouse retinal pigment epithelium. I. Cell and tissue morphometrics and topography of mitotic activity. *Dev. Biol.*, **121**, 192–204.
111. Stroeva, O.G. and Mitashov, V.I. (1983) Retinal pigment epithelium: proliferation and differentiation during development and regeneration. *Int. Rev. Cytol.*, **83**, 221–293.
112. Fuhrmann, S., Zou, C. and Levine, E.M. (2014) Retinal pigment epithelium development, plasticity, and tissue homeostasis. *Exp. Eye Res.*, **123**, 141–150.
113. Schouwey, K., Aydin, I.T., Radtke, F. and Beermann, F. (2011) RBP-Jkappa-dependent notch signaling enhances retinal pigment epithelial cell proliferation in transgenic mice. *Oncogene*, **30**, 313–322.
114. Defoe, D.M., Adams, L.B., Sun, J., Wisecarver, S.N. and Levine, E.M. (2007) Defects in retinal pigment epithelium cell proliferation and retinal attachment in mutant mice with p27 (Kip1) gene ablation. *Mol. Vis.*, **13**, 273–286.
115. Ma, X., Li, H., Wang, Y., Wang, J., Zheng, Q., Hua, J., Yang, J., Pan, L., Lu, F., Qu, J. *et al.* (2017) DAPL1, a susceptibility locus for age-related macular degeneration, acts as a novel suppressor of cell proliferation in the retinal pigment epithelium. *Hum. Mol. Genet.*, **26**, 1612–1621.
116. Yoshida, K., Nakayama, K., Kase, S., Nagahama, H., Harada, T., Ikeda, H., Harada, C., Imaki, J., Ohgami, K., Shiratori, K. *et al.* (2004) Involvement of p27 (KIP1) in proliferation of the retinal pigment epithelium and ciliary body. *Anat. Embryol.*, **208**, 145–150.
117. Schmidt, A., Tief, K., Yavuzer, U. and Beermann, F. (1999) Ectopic expression of RET results in microphthalmia and tumors in the retinal pigment epithelium. *Int. J. Cancer*, **80**, 600–605.
118. Chenn, A. and Walsh, C.A. (2002) Regulation of cerebral cortical size by control of cell cycle exit in neural precursors. *Science*, **297**, 365–369.
119. Cechmanek, P.B. and McFarlane, S. (2017) Retinal pigment epithelium expansion around the neural retina occurs in two separate phases with distinct mechanisms. *Dev. Dyn.*, **246**, 598–609.
120. Martinez-Morales, J.R., Cavodeassi, F. and Bovolenta, P. (2017) Coordinated morphogenetic mechanisms shape the vertebrate eye. *Front. Neurosci.*, **11**, 721.
121. Bokhovchuk, F., Mesrouze, Y., Izaac, A., Meyerhofer, M., Zimmermann, C., Fontana, P., Schmelzle, T., Erdmann, D., Furet, P., Kallen, J. *et al.* (2019) Molecular and structural characterization of a TEAD mutation at the origin of Sveinsson's chorioretinal atrophy. *FEBS J.*, **286**, 2381–2398.
122. Bouzas, E.A., Parry, D.M., Eldridge, R. and Kaiser-Kupfer, M.I. (1992) Familial occurrence of combined pigment epithelial and retinal hamartomas associated with neurofibromatosis 2. *Retina*, **12**, 103–107.
123. Hertwig, P. (1942) Neue Mutationen und Koppelungsgruppen bei der Hausmaus. *Z. Indukt. Abstamm. Vererbungsl.*, **80**, 220–246.
124. Hodgkinson, C.A., Moore, K.J., Nakayama, A., Steingrimsson, E., Copeland, N.G., Jenkins, N.A. and Arnheiter, H. (1993) Mutations at the mouse microphthalmia locus are associated with defects in a gene encoding a novel basic-helix-loop-helix-zipper protein. *Cell*, **74**, 395–404.
125. Mattapallil, M.J., Wawrousek, E.F., Chan, C.C., Zhao, H., Roychoudhury, J., Ferguson, T.A. and Caspi, R.R. (2012) The Rd8 mutation of the Crb1 gene is present in vendor lines of C57BL/6N mice and embryonic stem cells, and confounds ocular induced mutant phenotypes. *Invest. Ophthalmol. Vis. Sci.*, **53**, 2921–2927.
126. Chang, B., Hawes, N.L., Hurd, R.E., Davisson, M.T., Nusinowitz, S. and Heckenlively, J.R. (2002) Retinal degeneration mutants in the mouse. *Vis. Res.*, **42**, 517–525.
127. Mehalow, A.K., Kameya, S., Smith, R.S., Hawes, N.L., Denegre, J.M., Young, J.A., Bechtold, L., Haider, N.B., Tepass, U., Heckenlively, J.R. *et al.* (2003) CRB1 is essential for external limiting membrane integrity and photoreceptor morphogenesis in the mammalian retina. *Hum. Mol. Genet.*, **12**, 2179–2189.